

U-Pb LA-(MC)-ICP-MS dating of rutile: new reference materials and applications to sedimentary provenance

Laura Bracciali^{a,b,*}

Randall R. Parrish^{a,c}

Matthew S.A. Horstwood^a

Daniel Condon^a

Yani Najman^b

^a NERC Isotope Geosciences Laboratory, British Geological Survey, Keyworth, Nottingham, United Kingdom

^b Lancaster Environment Centre, Lancaster University, Lancaster, United Kingdom

^c Department of Geology, University of Leicester, Leicester, UK

* Corresponding author at: NERC Isotope Geosciences Laboratory, British Geological Survey, Keyworth, Nottingham, NG12 5GG, UK. Tel: +44 (0)115 9363278.

E-mail address: laur@bgs.ac.uk (L. Bracciali).

Abstract

In response to the general lack of sufficiently abundant and high quality rutile U-Pb reference materials for in situ geochronology, we have characterised two new potential rutile ~ 1.8 Ga reference materials (Sugluk-4 and PCA-S207) from granulite facies belts of the Canadian Shield, namely the northern Cape Smith Belt of Quebec and the Snowbird Tectonic Zone (Sasatchewan). Characterisation includes ID-TIMS and LA-ICP-MS U-Pb dating, imaging, and trace element analysis. We compare these materials with existing rutiles used already (R19 and R10; Luvizotto et al., 2009; Zack et al., 2011) and show that the measured U-Pb compositions (i.e. including any common Pb) of our rutiles are considerably more homogeneous. This makes possible a U-Pb normalisation procedure (not reliant upon a common Pb correction) that results in a significant decrease in the uncertainty contribution from the common Pb correction and better reproducibility of reference materials and

unknowns for provenance analysis and other applications. The reproducibility is 2–4% (2RSD) for $^{206}\text{Pb}/^{238}\text{U}$ and $^{207}\text{Pb}/^{206}\text{Pb}$, only slightly greater than long-term data for zircon reference materials. We show in a rutile provenance study from young orogens (Bhutan Himalaya and Canadian Cordillera) that the sensitivity of our analytical set-up allows dating of ~90% of rutiles in a sediment using a 50 μm laser ablation spotsize within samples containing rutile as young as 10–20 Ma, and obviates the requirement for U concentration pre-screening, thus reducing or eliminating rutile selection bias. Unsuccessful analyses are due to poor quality rutiles with predominant common Pb, ^{207}Pb signal below detection, or U content below ~1-2 ppm. We have used the ‘ ^{207}Pb -method’ (using the Tera-Wasserburg diagram) to correct for substantial common Pb in very young and/or very low-U rutiles, rather than developing an on-line correction. Since rutile ages reflect mainly the time of cooling, rutile is a sensitive recorder of metamorphic thermochronological information and therefore is an excellent complement to detrital zircon U-Pb data. The contrast between zircon and rutile signatures in Himalayan samples with rutile as young as 10 Ma is shown to be very dramatic (most zircons from the same sample are > 480 Ma, with only a few grains or metamorphic rims reflecting Miocene metamorphism); as such rutile provides complementary information about the thermal events within the source regions of the grains. Rutile U-Pb dating is an underexploited provenance method with wide applicability to sedimentary provenance studies.

Keywords

Rutile U-Pb dating, LA-MC-ICP-MS, detrital thermochronology, sedimentary provenance, Sugluk-4, common Pb correction

1. Introduction

Rutile, the most common polymorph of TiO_2 , is a widely distributed accessory mineral in medium- to high-grade metamorphic and some igneous, chiefly plutonic, rocks. Due to its chemical and physical stability during the sedimentary cycle, rutile is commonly found in the heavy mineral suite of sedimentary rocks and can therefore provide important information about provenance. Rutile typically consists of > 98 wt % TiO_2 , but considerable amounts of other elements such as Fe, Cr, Nb and Ta and other HFSE (high field strength elements) can enter the crystalline lattice, allowing insight into rock forming conditions and discrimination between different source lithologies in provenance studies (e.g., Zack et al., 2004a; Carruzzo et al., 2006; Triebold et al., 2007; Meinhold et al., 2008; Morton and Chenery, 2009; Ewing et

al., 2011; Meyer et al., 2011). The Zr content of rutile crystallised in a zircon-saturated environment is strongly dependent on temperature (Zack et al., 2004b; Watson et al., 2006; Ferry and Watson, 2007; Tomkins et al., 2007), and Zr-in-rutile is used as a geothermometer, commonly coupled to the Ti-in-zircon thermometer. Uranium can be easily accommodated in the crystalline structure of rutile due to the comparable ionic radius and charge to Ti^{4+} , hence rutile can be dated by the U-Pb method, but it has comparatively received far less attention than zircon perhaps due to its usually lower U concentration (from as low as < 0.01 ppm to ~ 100 ppm) and to the lack of rutile mineral reference materials needed for microprobe dating. However, rutile has been used for some years by the ID-TIMS (isotope dilution thermal ionisation mass spectrometry) community for high precision dating via the U-Pb system. For further reading on rutile properties and applications in the earth sciences the reader is referred to Meinhold (2010).

The radiogenic Pb content of rutile is a function of the time since it cooled below its closure temperature (T_C) and accumulated Pb due to the radioactive decay of U. When this T_C is lower than the crystallisation temperature (Dodson, 1973) the measured age represents the time of cessation of Pb volume diffusion during cooling. T_C is a function of diffusivity, cooling rate, and effective diffusion radius. Mezger et al. (1989) used ID-TIMS to date rutile grains from amphibolite to granulite facies metapelitic rocks, and compared the results to dates obtained for other minerals with reasonably well-known T_C (zircon, garnet, sphene, monazite, as well as hornblende and biotite dated by the K-Ar and $^{40}\text{Ar}/^{39}\text{Ar}$ method). This empirical calibration resulted in T_C estimates for rutile of 380 and 420 °C depending on grain size of crystals (respectively 70–90 and 90–210 μm). These estimates were later upwards-revised to 500 and 540 °C (for rutile with diameter 140–180 and 180–420 μm ; Vry and Baker, 2006). Based on diffusion experiments over the range 700–1100 °C on natural and synthetic rutile with significant differences in trace element composition, Cherniak (2000) calculated mean T_C of ~ 600 °C for rutile grains of ~ 100 μm size. Observed age heterogeneity, determined by LA-ICP-MS (laser ablation inductively coupled plasma mass spectrometry), within relatively large grains (up to 280 μm in size) from granulite facies Archean metapelitic rocks showing systematic core-to-rim decrease of several tens of millions of years (640 to 510°C) and increase in age-gradient, lead Kooijman et al. (2010) to interpret the intragrain U-Pb variations as cooling ages recording points in time where the system effectively closed for Pb, and to construct closure temperature profiles ($T_C(x)$, Dodson, 1986) across the grains. U-Pb dates obtained for rutile are younger than coexisting zircon and represent the time of

cessation of Pb volume diffusion during cooling below ~ 500 °C; rutile can thus be used as a thermochronometer in studies aimed at constraining the timing of metamorphism or the thermal evolution of igneous and metamorphic terranes (Schärer et al., 1986; Corfu and Muir, 1989; Mezger et al., 1989; Flowers et al., 2005; 2006; Storey et al. 2007; Kylander-Clark et al., 2008; Li et al., 2011; Blackburn et al., 2011, 2012). Growing interest is also being paid to U-Pb chronology of detrital rutile as a provenance indicator (Allen and Campbell, 2007; Birch et al., 2007; Rösel et al., 2011; Meinhold et al., 2011; Okay et al., 2011). While U-Pb chronology of rutile by ID-TIMS is a well established technique and allows high precision ratios to be measured (e.g., Ludwig and Cooper, 1984; Schärer et al., 1986; Corfu and Andrews, 1986; Mezger et al., 1989; Davis, 1997; Cox et al., 2002; Treloar et al., 2003; Schmitz and Bowring, 2003), rutile can also be dated by microprobe (secondary ion mass spectrometry – SIMS, LA-ICP-MS) techniques (Sircombe, 1995; Clark et al., 2000; Vry and Baker, 2006; Harrison et al., 2007; Storey et al., 2007; Kooijman et al., 2010; Meinhold et al., 2011; Zack et al., 2011; Schmitt and Zack, 2012; Taylor et al., 2012).

A potential issue for U-Pb dating of rutile, especially in young, less radiogenic samples, is the relatively large proportion of common (non radiogenic) Pb (i.e., which can be incorporated into the crystal structure during crystallisation or derived from contamination) resulting in low ratios of radiogenic Pb to common Pb (e.g., Treloar et al., 2003 from UHP rocks). The problem has been variably addressed, most commonly by assessing the common Pb composition at the time of crystallisation using multiple analyses of rutile and mineral isochrons, or by assuming a model-based composition of common Pb using measured ^{204}Pb in the same mineral, or by applying a correction for the common Pb content following the determination of the common Pb composition as measured in a (U-Th poor) mineral coexisting in the same rock, the latter method not being applicable to detrital samples. Alternatively, making use of the observation that rutiles contain very low Th (hence negligible radiogenic ^{208}Pb from ^{232}Th decay), the measured isotopic ratios can be corrected for common Pb by measuring ^{208}Pb and assuming it is virtually entirely common Pb (Clark et al., 2000; Allen and Campbell, 2007; Kooijman et al., 2010; Zack et al., 2011). Currently, strategies are not available for handling reference material data with variable common-Pb to determine normalisation factors for LA U-Pb dating. In the absence of this, data must first be corrected for common-Pb using one of the above approaches. However, the routine application of a common Pb correction and the necessary uncertainty propagation, risks masking scatter in the reference material data which may or may not be relevant to the nature

of the sample analysis. Equally, correction and propagation of the sample datapoints may mask the resolution of further age scatter. In addition to the inability of some instrumental set-ups to measure precisely some relevant isotopes (e.g. ^{204}Pb , ^{208}Pb), the problem of determining normalisation factors from data with variable common Pb and the additional uncertainty contribution, makes favourable the use of a reference material without significant common-Pb if one could be found. In this study, U-Pb dating by LA-MC-ICP-MS is applied to detrital rutile and two new natural rutile materials (Sugluk-4 and PCA-S207) are presented as primary and secondary reference materials to use during analysis, for which high precision ID-TIMS U-Pb and abundant LA U-Pb dates have also been determined. An approach of reference material and sample analysis is developed and presented that can be applied to the wider challenge of detrital rutile single grain U-Pb dating for provenance studies. Our approach benefits from the use of multi-collector ICP-MS which typically exhibit better detection efficiencies than single-collector sector-field or quadrupole-ICP-MS techniques as well as simultaneous measurement of ion beams resulting in higher precisions for equivalent analysis durations (or the use of shorter acquisition times and lower ablation volumes whilst achieving equivalent precision). This allows accurate determination of the vast majority of rutiles in a sediment (> 75 and 90 % on average, using a 35–40 or 50 μm spot size, respectively, based on 16 modern river sand samples 6 of which are shown in this study) without requirement for concentration pre-screening which might serve to bias the population distribution. We show that our reference materials are near-concordant with a low relative common Pb content and a long-term reproducibility only modestly worse than long-term data for zircon reference materials. This eliminates the necessity for a common Pb correction to be applied to the reference data before establishing the U/Pb normalisation value as well as the uncertainty propagation which would also be necessitated. Due to the lower T_C of rutile compared to zircon, rutile has the potential to become a key tracer in sedimentary provenance, especially in combination with zircon, as together they provide a better defined isotopic fingerprint of the source region. Additionally, the availability of good quality reference materials will favour the application of U-Pb dating of detrital rutile in provenance studies in the future.

2. Rutile reference materials

Two rutile samples from granulite facies metasedimentary rocks, Sugluk-4 (Sugluk-4-87 of Parrish, 1989) and PCA-S207 (PCA-S207-90-A), were chosen as candidate reference materials due to their abundance, general lack of inclusions and their age and tectonic setting.

One of our objectives was to identify materials of sufficient quantity, quality and suitability in order to be able to distribute aliquots of both materials to other laboratories on request. The two rutile samples consist of gram-quantities that generally fall in a grain size range of 100–500 μm . Sugluk-4 is a granulite facies quartzite from the Ungava segment of the Trans-Hudson orogen of Canada (Sugluk-4) and PCA-S207 is a highly strained granulite facies paragneiss (“upper deck diatexite” of Hanmer et al., 1994) from the East Lake Athabasca region (Canada). The exact geographical coordinates are indicated in Table 1 and further details on the geological and metamorphic setting of these samples (not necessarily relevant to their use as reference materials) can be found in the Supplementary data file. The garnet-bearing paragneiss PCA-S207 is a leucocratic banded rock with 0.2 to 3 mm thick ribbons of quartz alternating to granular layers of quartz and alkali feldspar, with minor twinned plagioclase. The planar fabric wraps around 1 to 5 mm garnet porphyroclasts colourless in thin section. Reddish brown rutile 0.1 to 0.5 mm across is a relatively abundant accessory phase. Sample Sugluk-4 is an isotropic quartzite made of large (up to a few cm) quartz domains with irregular contacts and minor interstitial sericitized feldspar domains with relics of crosshatched twinning. Isolated white mica flakes (~ 1 mm) are present. Rutile is rarely observed in thin section. Images of PCA-S207 and Sugluk-4 rutile grains are shown in Fig. 1. The grains range in size from a few tens μm to several hundreds μm , are translucent and brown-red to dark-brown, with Sugluk-4 grains idioblastic to sub-idioblastic (Fig. 1a), while PCA-S207 grains are commonly xenoblastic (Fig. 1i). Colour zoning is rare. In thin section the grains are reddish brown (Figs. 1b, d, e, l, n, o) and can show twinning (e.g. Fig. 1c). BSE imaging did not reveal zonation patterns (Figs. 1f, g, h, q, r, s).

3. Analytical methods for reference material characterisation

Rutile grains were isolated from the samples by mineral separation techniques making use of standard crushing, milling, dense liquid separation and Frantz magnetic separation. In characterising the rutiles, typical grains were selected, mounted in epoxy resin and polished to expose their interiors. The characterised grains are representative of rutile grains from the separates and are not specially selected.

3.1 ID-TIMS U-Pb dating

ID-TIMS U-Pb dates of rutile were measured at the NERC Isotope Geosciences Laboratory (NIGL), British Geological Survey, UK. Single rutile crystals or fragments were hand-picked, photographed (in transmitted light) and rinsed (in ultrapure acetone) prior to being transferred

to 300 µl Teflon FEP microcapsules and spiked with a mixed ^{233}U - ^{235}U - ^{205}Pb tracer. Rutile was dissolved in ~ 120 µl of 29 M HF with a trace amount of 30% HNO_3 with microcapsules placed in Parr vessels at ~ 220°C for > 60 hours; total dissolution was checked by visual inspection during each dissolution batch. Solutions were dried to fluorides, and then converted to chlorides at ~ 180 °C overnight. U and Pb for all minerals were separated using standard HBr-HCl based anion-exchange chromatographic procedures.

Isotope ratios were measured using a Thermo-Electron Triton thermal ionisation mass-spectrometer (TIMS). Pb and U were loaded together on a single Re filament in a silica-gel/phosphoric acid mixture (Gerstenberger and Haase, 1997). Pb was measured by peak-hopping on a single SEM detector. U isotopic measurements were made in static Faraday mode. Age calculation and uncertainty estimation (including U/Th disequilibrium) was based upon the algorithms of Schmitz and Schoene (2007).

3.2 LA-MC-ICP-MS U-Pb dating

Laser ablation U-Pb data were collected using either a 193 nm or a 213 nm wavelength laser ablation system (UP193SS, UP193FX and UP213SS, New Wave Research) coupled to a Nu Plasma HR multiple-collector inductively coupled plasma mass spectrometer (MC-ICP-MS, Nu Instruments). The mass spectrometer used has a specially designed collector block to allow simultaneous detection of all masses in the range 202–207, 235 and 238. Methods followed those described in Thomas et al. (2010) with the data reduction and uncertainty propagation methodologies described in Horstwood et al. (2003). Instrument parameters used during analysis are detailed in Table A (Supplementary data file). Either a low-volume (volume ~ 3 cm³, Horstwood et al., 2003) or a two-volume (Large Format Cell of New Wave Research) ablation cell were used for sample analysis. The laser sampling protocol employed a 35, 40 or 50 µm static spot – depending on crystal size – and a fluence of 2–3 J/cm² (independently calibrated). Analysis was performed using the Time Resolved Analysis (TRA) mode of the Nu Plasma software with signals integrated excluding the first 3–5 s of data and the data normalised and uncertainty propagated offline using an in-house Excel spreadsheet. After an initial 30 s instrument baseline measurement and 30 s gas blank, individual analysis ablation times were 40 s for a run of 10–15 ablations. Average pit depth estimates of ~ 20 µm were confirmed by independent SEM measurements on a few grains (Fig. 2). Ion beams for mass 204 (Pb and Hg), ^{206}Pb and ^{207}Pb were collected on ETP discrete dynode electron multipliers with all other peaks collected on analogue (Faraday) detectors. The simultaneous measurement of the ^{202}Hg signal allows correction for the isobaric interference of ^{204}Hg on

^{204}Pb during the ablation. Detection of very small amounts of ^{204}Pb is however currently hampered by the quantity of Hg in the gas blank, leading to a relatively high on-peak subtracted noise level on ^{204}Pb , masking the low ^{204}Pb signals typical of many rutile ablations and ultimately leading to poor precision on small common Pb corrections. A desolvating nebuliser (DSN-100, Nu Instruments) was used to simultaneously aspirate a solution containing Tl (with isotopes 203 and 205) and ^{235}U in order to correct for mass spectrometer-related mass bias (Pb/Pb ratios using $^{205}\text{Tl}/^{203}\text{Tl}$, Pb/U ratios using $^{205}\text{Tl}/^{235}\text{U}$) at the time of analysis. Elemental fractionation from other sources (laser- and plasma-induced) was corrected by comparison of laser ablation data for a primary reference material to ID-TIMS data. In line with best practice in laser ablation analysis, at least one secondary reference material is required to validate the results and assess the quality of the U-Pb data, hence both reference rutiles were analysed in each session, one to provide validation for the corrections determined from the other. Uncertainties for the $^{207}\text{Pb}/^{206}\text{Pb}$ ratios were propagated using quadratic addition to combine the measurement uncertainty with a reproducibility component modelled to reflect increasing uncertainty with decreasing signal size (see Horstwood et al., 2003 for details). A minimum uncertainty of 0.5% (2σ) was assigned to the $^{207}\text{Pb}/^{206}\text{Pb}$ ratio by default for ablations with high ^{207}Pb ion beams, to reflect the confidence in the ability of the multi-ion counting (MIC) set-up to accurately reproduce any one value. $^{206}\text{Pb}/^{238}\text{U}$ uncertainties were propagated in a similar way utilising the measurement uncertainty and the reproducibility of the ablation reference material used. During each analytical session both zircon and rutile reference materials were measured between each group of unknowns to determine the degree of elemental fractionation, to monitor the effect of matrix (zircon vs. rutile) on the degree of elemental fractionation, and to assess instrumental accuracy. GJ-1 zircon reference material ($^{206}\text{Pb}/^{238}\text{U}$ age = 600.4 ± 0.6 Ma, Jackson et al., 2004; 602.3 ± 1 Ma NIGL TIMS data unpublished) was used as the primary zircon reference material with Mud Tank (732 ± 5 Ma, Black and Gulson, 1978) and 91500 (1062.4 ± 0.4 Ma, Wiedenbeck et al., 1995) or Plešovice (337.1 ± 0.4 Ma, Sláma et al., 2008) as secondary zircon reference materials. Sugluk-4 and PCA-S207 were analysed as primary and secondary rutile reference materials respectively. The weighted means of the $^{207}\text{Pb}/^{206}\text{Pb}$ and $^{206}\text{Pb}/^{238}\text{U}$ Sugluk-4 ratios obtained by ID-TIMS (without correction for common Pb) were used as the reference values to determine the normalisation factors relative to the average $^{207}\text{Pb}/^{206}\text{Pb}$ and $^{206}\text{Pb}/^{238}\text{U}$ (after mass-bias correction (mbc) using the Tl-U solution) obtained over the course of each LA-MC-ICP-MS analytical session. These factors were used to normalise the data for the

validation (PCA-S207) and sample analyses. All plots and age calculations have been made using the Isoplot v. 4.14 (Ludwig, 2003) add-in for Microsoft Excel.

3.3 Determination of trace element composition by LA-ICP-MS

Laser ablation ICP-MS was used to determine the trace element content of rutile grains from Sugluk-4 and PCA-S207. Element concentrations were measured at the University of Portsmouth using an Agilent 7500cs quadrupole ICP-MS coupled to a New Wave UP213 laser ablation sampling system. Helium was used as a carrier gas and mixed with Ar via a connector prior to the torch. Spots were located as close as possible to the spots used for LA U-Pb dating. Data were collected using a 60 s acquisition and backgrounds were measured as a gas blank for the first 30 s. The spot size was 40 μm with a repetition rate of 10Hz and laser fluence was maintained at $\sim 4 \text{ J/cm}^2$. NIST SRM 610 glass (Pearce et al., 1997) was used as the reference material for concentration determination, to correct for elemental fractionation and mass bias and was measured at the beginning and end of data acquisition and between each group of 14 unknowns. Internal standardisation was done stoichiometrically by assuming $\text{TiO}_2 = 98 \text{ wt\%}$ in rutile. Oxide formation was kept below 0.1% by monitoring Th/ThO^+ . Rutile R10 was monitored within each run and checked against the published values of Luvizotto et al. (2009). The data were reduced offline using Lamtrace (Simon Jackson, Geological Survey of Canada). All of the elements analyzed were reproduced to within 4 and 9 % (1σ), with the exception of Al and W (20 %), on the basis of long-term reproducibility.

4. Reference materials results

4.1 Mineral chemistry

Selected typical Sugluk-4 and PCA-S207 rutile grains were analysed for chemical composition and intragrain variability, as tested by ablating different areas of individual grains (e.g., Figs. 1h and 1s; Table 1). A selection of elements in the mass range 27–238 was measured by LA-ICP-MS, with many being below the detection limit of the technique (e.g., Mn, Rb, Sr, Y, the Rare Earth Elements; these are not included in Table 1). The most abundant trace elements (in the range of hundreds to a few thousand ppm) are Zr, Cr, Nb and V. The concentrations of the trivalent elements Sc and Al differ in Sugluk-4 and PCA-S207 rutiles with PCA-S207 enriched in Al and Sugluk-4 in Sc (Fig. 3a). The HFSE (High Field Strength Elements, such as Zr, Nb, Mo, Sn, Hf, Ta, W) of which rutile is a main carrier mineral phase (e.g., Rudnick et al., 2000) occur in variable amounts in the analysed grains. Zr and Hf show broad positive correlations, and form two distinct trends for Sugluk-4 (lower

Zr/Hf) and PCA-S207 (higher Zr/Hf, Table 1 and Fig. 3b). Nb occurs with concentrations up to ~ 2000 ppm and is more homogeneously distributed in Sugluk-4 than in PCA-S207 (Fig. 3c). The Nb/Ta ratio of PCA-S207 and Sugluk-4 varies in the range 9–62 and 15–78, respectively (Table 1 and Fig. 3c). Cr and V are broadly positively correlated (Fig. 3d). Sugluk-4 is also characterized by less variable Cr/Nb ratios (0.5–1) than PCA-S207 (0.5–3, Table 1 and Fig. 3e). The measured U concentration is in the range 12–40 and 24–98 ppm in PCA-S207 and in Sugluk-4 respectively (Fig. 3f), while Th occurs below an average detection limit of ~ 0.001 ppm. For a few grains for which U-Pb isotopes had been measured by LA-MC-ICP-MS on a corresponding spot, the Pb concentration has been calculated using the measured U concentration and is 5 to 9 ppm (PCA-S207) and 8 to 30 ppm (Sugluk-4), (Table 1). The higher U and Pb content in Sugluk-4 is also confirmed by the U and Pb content estimated on the basis of GJ1 zircon analysed in the same LA U-Pb session, with an average of 7 (Pb) and 17 (U) ppm for PCA-S207, 11 (Pb) and 30 (U) ppb for Sugluk-4 (Table D, Supplementary data file). Overall, Sugluk-4 is a more chemically homogeneous material than PCA-S207. In some grains and for some elements (e.g. Nb, Ta, Zr, Hf) some intragrain chemical variability can be observed (e.g. Figs. 3g to 3l). Temperatures calculated applying the Zr-in-rutile thermometer (based on the calibration of Tomkins et al., 2007) are in the range of 700–760 °C (assuming a P of 6 kbar) and 710–780 °C (10 kbar) for Sugluk-4 and 680–770 °C (6 kbar) and 700–790 °C (10 kbar) for PCA-S207, consistent with granulite facies conditions of the two rutiles (Table 2).

4.2 U-Pb isotopic results

4.2.1 ID-TIMS

Rutile ID-TIMS U-Pb data for ten Sugluk-4 and four PCA-S207 individual grains are presented in Table 3, along with analyses of four fragments of the R10 monocrystalline rutile (Luvizotto et al., 2009). The results, both before and after correction for common Pb, are plotted on Wetherill concordia diagrams (Fig. 4). The data for Sugluk-4 (Table 3 and Fig. 4a) detail the presence of small amounts of common Pb (0.2–1.6% for 8 of 10 analyses). After common Pb correction (using the Stacey-Kramers (1975) model for terrestrial Pb evolution at 1.7 Ga), the data form a co-linear array regressing to near-zero age with an upper intercept age of 1723.0 ± 6.8 Ma (2σ , including decay constant uncertainties, MSWD = 11, excluding one point). However the exact interpretation of rutile ages is complicated and this will be discussed later. Importantly, the average $^{206}\text{Pb}/^{238}\text{U}$ and $^{207}\text{Pb}/^{206}\text{Pb}$ ratios differ by <1% for 8 of the 10 grains whether or not they are corrected for common Pb (Fig. 4a). This level of

potential inaccuracy is currently appropriate for LA-ICP-MS dating for a mineral with limited available alternative reference materials. On the scale of current laser ablation uncertainties (2%, 2σ) therefore, it makes little difference whether the ID-TIMS common Pb corrected or non-corrected $^{206}\text{Pb}/^{238}\text{U}$ and $^{207}\text{Pb}/^{206}\text{Pb}$ ratios of Sugluk-4 are used as the primary reference values for normalising the laser ablation data. For materials with a higher relative common Pb content (e.g. R10, see later) this difference is important and requires like-for-like data normalisation if used as a primary reference material. With this in mind and the knowledge that age variations related to cooling are present and normal in many rutiles, the Sugluk-4 (radiogenic plus common Pb) $^{206}\text{Pb}/^{238}\text{U}$ and $^{207}\text{Pb}/^{206}\text{Pb}$ ratios for normalisation of the LA data were defined as $0.3060 \pm 2\%$ and $0.1070 \pm 1.4\%$ (2RSD), respectively

Four PCA-S207 rutile grains show higher relative common Pb contents of 2.9–45% compared to Sugluk-4, the very high relative common Pb content of one grain possibly due to an inclusion of another mineral. The four points do not form a co-linear common Pb array and after common Pb correction are not equivalent (Figs. 4b and 4c). The average PCA-S207 $^{206}\text{Pb}/^{238}\text{U}$ and $^{207}\text{Pb}/^{206}\text{Pb}$ ratios for the common Pb corrected data are $0.3303 \pm 1.8\%$ and $0.1141 \pm 0.5\%$ (2RSD).

Four fragments of the 1090 Ma R10 rutile (Luvizotto et al., 2009) analysed by ID-TIMS contained 0.24–1.6% common Pb and were concordant after correction, but only 3 of the 4 analyses overlap at the 2σ level; these data overlap with the bottom end of the data cluster published by Luvizotto et al (2009), (Fig. 4d). R10 was introduced and characterised by Luvizotto et al. (2009) and used as reference materials for U-Pb dating by Zack et al. (2011), therefore it is important to undertake some intercomparison of our proposed reference materials with that. Since we are not applying an online common Pb correction during the analysis, data values prior to common Pb correction need to be determined in order to use R10 as the main reference material. This also requires the reference material to have homogenous radiogenic Pb to common Pb ratios throughout. Using the published *radiogenic* ratios of fourteen R10 fragments (Table 4 of Luvizotto et al., 2009) we have back-calculated the $^{207}\text{Pb}/^{206}\text{Pb}$ and $^{206}\text{Pb}/^{238}\text{U}$ ratios prior to common Pb correction by adding a common Pb component (quantified by the $^{206}\text{Pb}/^{204}\text{Pb}$ of their Table 4) with a composition calculated at 1090 Ma using the Stacey-Kramers (1975) model for terrestrial Pb evolution (Table B, Supplementary data file). These are plotted on a Wetherill concordia diagram along with the R10 fragments measured in this study (Fig. 4e). With $^{206}\text{Pb}/^{204}\text{Pb}$ ratios of 330 to 4000 with most being less than 1000, R10 is clearly not appropriate for our purposes as a reference

material prior to common Pb correction. In addition, based on Fig. 4e, it is possible that the two sets of data do not lie on the same regression trend indicating that there are variable age and/or common Pb components within R10. For our purposes therefore, and for others who do not or prefer not to measure ^{204}Pb and/or ^{208}Pb , R10 can not serve as a primary reference material.

4.2.2 LA-MC-ICP-MS

Rutile LA-MC-ICP-MS U-Pb data were acquired over a period of ca. two years (29 analytical sessions for a total of ~ 2500 single ablations, including 1800 ablations of grains from 26 unknown detrital samples; six of these detrital samples are presented in this paper -section 5- to show our approach on real samples). Over the ~ 2 year period of our LA U-Pb rutile measurements and during the same analytical sessions we also measured three commonly-used zircon reference materials (Table C, Supplementary data file). The long-term reproducibility (2RSD) of the $^{207}\text{Pb}/^{206}\text{Pb}$ and $^{206}\text{Pb}/^{238}\text{U}$ ratios for the secondary zircon reference materials normalised to GJ1 (Figs. 5b to 5c) over the same period was 2.0 and 3.0% for Mud Tank ($n = 157$), 1.5 and 3.3% for Plešovice ($n = 25$), 1.8 and 2.6% for 91500 ($n = 106$). These data demonstrate that instrument performance during this period was good. Sugluk-4 rutile LA U-Pb data (486 spot ablations on 72 grains; Table D, Supplementary data file) are plotted on a Tera-Wasserburg diagram along with the ID-TIMS analyses of individual grains (Fig. 5a, all data not corrected for common Pb). The Sugluk-4 $^{207}\text{Pb}/^{206}\text{Pb}$ ratios not corrected for common Pb exhibit an asymmetric probability density distribution with a positive skew (Fig. 6a). The same data are shown as linearised probability plot (Fig. 7a) after the exclusion of datapoints with $^{207}\text{Pb}/^{206}\text{Pb} > 0.11$ (14 out of 486, i.e. 3%), under the assumption that these higher ratios reflect the occurrence of common Pb despite this being below a level detectable with our analytical set-up. On the linearised probability plot the main set of data disperse along a linear trend with a slope of ~ 1 as a normal distribution would do. The $^{206}\text{Pb}/^{238}\text{U}$ distribution (of the 486 datapoints) also exhibits a skew, as shown by the probability density plot in Fig. 6b. Excluding the same 14 data points with higher relative common Pb as excluded in Fig. 7a, the residual scatter in $^{206}\text{Pb}/^{238}\text{U}$ ratio shown by the linearised density plot (Fig. 7b) but not evident in $^{207}\text{Pb}/^{206}\text{Pb}$ space (Fig. 7a), is caused by 13 analyses of the remaining 472 with anomalously high $^{206}\text{Pb}/^{238}\text{U}$. The origin of this is currently unknown although is likely to be real variation arising from the protracted cooling history of the sample. The $^{207}\text{Pb}/^{206}\text{Pb}$ average of the 472 datapoints illustrated as a linearised probability plot (Fig. 7a) is 0.1069 ± 0.0021 (2.0%, 2SD). The $^{206}\text{Pb}/^{238}\text{U}$ average of 459

datapoints illustrated as a linearised probability plot (Fig. 7c) is 0.306 ± 0.011 (3.6%, 2SD). This long-term reproducibility of the $^{207}\text{Pb}/^{206}\text{Pb}$ and $^{206}\text{Pb}/^{238}\text{U}$ ratios for Sugluk-4 is equal to or slightly worse than that of zircon reference materials analysed over the same period (1.5 to 2.0% and 2.6 to 3.3% respectively). However, the same individual rutile grain ablated over different analytical sessions or different grains analysed within the same session are more reproducible (e.g. note the $^{206}\text{Pb}/^{238}\text{U}$ reproducibility dropping to $< 3\%$ in Figs. 7d and 7e) suggesting that inter-grain variation combined with session-to-session scatter are the controlling factors on data homogeneity.

Allowing for natural variations induced by protracted cooling and assuming no Pb loss in rutile our best estimate for the age of Sugluk-4 is 1719 ± 14 Ma (the average and 2SD of 8 out of ten ID-TIMS data, see section 4.2.1). It is important to note, however, that slow cooling and related diffusion will inevitably induce some intragrain and intergrain age variation (e.g. Baldwin et al., 2004; Flowers et al., 2006; Kooijman et al., 2010) and that in some grains this would be measurable leading to a preferred age different to the one stated. With a sufficiently high sample quantity, this may appear in a dataset as a slight heterogeneity, consistent with what has been observed. In light of this natural variation, the $^{207}\text{Pb}/^{206}\text{Pb}$ and $^{206}\text{Pb}/^{238}\text{U}$ ratios used to represent Sugluk 4 are therefore an average based on the ID-TIMS data with an uncertainty assigned (2.0% and 3.6%, 2SD) which allows for this variation and provides a limiting uncertainty in the interpretation of the data. Data reported by Zack et al. (2011) for R10 cite *within run* reproducibility at 3.5% (2SD). Therefore, using Sugluk-4 as a primary reference material results in limiting uncertainties equivalent to R10.

PCA-S207 LA U-Pb data (normalised to Sugluk-4 and not corrected for common Pb, 412 spot ablations on 85 grains; Table D, Supplementary data file) are shown in Fig. 8a as a Tera-Wasserburg diagram, along with the ID-TIMS analyses of individual grains. The same LA U-Pb data are shown as probability plots (Figs. 8b and 8c) and as linearised probability plots after the exclusion of datapoints with $^{207}\text{Pb}/^{206}\text{Pb} > 0.122$ (14 out of 400, i.e. 4%), under the assumption that these higher ratios are due to common Pb at the limits of detection for our analytical set-up. Similarly to Sugluk-4, there is a residual scatter that can be explained in terms of either Pb loss or more likely the effects of the protracted cooling that may have caused some real intergrain variation. This is reflected in the data populations in Figs. 8b and 8c being clearly non-normally distributed. Here the cooling history of PCA-S207 might be responsible for the larger variability of the $^{207}\text{Pb}/^{206}\text{Pb}$ and $^{206}\text{Pb}/^{238}\text{U}$ ratios compared to Sugluk-4. Nonetheless, the intragrain or short term (daily) variability of PCA-S207 is usually

below 4.0 % (2σ) for both ratios. Our best estimate for the age of PCA-S207 rutile is 1865.0 ± 7.5 Ma (weighted average of $^{207}\text{Pb}/^{206}\text{Pb}$ ID-TIMS dates, based on four concordant to nearly concordant grains ranging from 1862.2 ± 2.8 to 1872.2 ± 2.6 . 95% conf., MSWD = 13); this is in good agreement with $^{207}\text{Pb}/^{206}\text{Pb}$ rutile dates in the range 1850.8 ± 1.4 to 1881.6 ± 2.4 Ma and 1874.0 ± 1.0 to 1892.9 ± 5.8 Ma from an eclogite and the Axis mafic granulite from the southern domain of the East Atabasca Mylonite triangle (ID-TIMS data, 6 grains each; Baldwin et al., 2004; Flowers et al., 2006) from where PCA-S207 has been sampled (see Geological and thermochronological setting, Supplementary data file). Interestingly Baldwin et al. (2004) noticed an age-correlation with grain size and interpreted it as differential closure to diffusion, and Flowers et al. (2006) argued for intracrystal variation in age that may reflect diffusional gradients developed during cooling. Our conclusions are therefore similar using the two different methods (ID-TIMS and LA-MC-ICP-MS).

In order to undertake some intercomparison of our proposed reference materials with R10 and R19 (Luvizotto et al., 2009; Zack et al., 2011), fragments of these two rutiles were ablated along with Sugluk 4 and PCA-S207 during some of the same analytical sessions. Due to the large variability in common Pb content in R10 highlighted in the Luvizotto et al (2009) ID-TIMS data (> 50% variability in $^{207}\text{Pb}/^{206}\text{Pb}$ ratio), each individual fragment of R10 requires knowledge of its isotopic composition and homogeneity to be used as a primary reference material. In the absence of an on-line common Pb correction being applied to data, a homogeneous or common Pb-free material is required as a primary reference. Some of the data of R10 in Luvizotto et al (2009) exhibits relatively low common Pb (Table 4 of Luvizotto et al., 2009). The R10 data from this study demonstrate a lower relative common Pb content of the data than have been published so far. Using an average of these (filled ellipses of Figs. 4d and 4e) for normalisation of R19 and PCA-S207 ablated as unknown materials (Fig. 9a and 9c) concordant data are achieved (excluding two R19 discordant datapoints with higher relative common Pb content). The weighted average $^{206}\text{Pb}/^{238}\text{U}$ date for R19 is 472.6 ± 6.5 (9 datapoints concordant and equivalent within uncertainty, Fig. 9a), while the published weighted average of four TIMS $^{206}\text{Pb}/^{238}\text{U}$ dates for R19 is 489.5 ± 0.9 Ma (Zack et al., 2011). Using Sugluk-4 as the primary reference material, the same level of concordance results for R19 datapoints, and the weighted average $^{206}\text{Pb}/^{238}\text{U}$ date is 470.1 ± 4.9 Ma (Fig. 9b) within uncertainty of that for the R10 normalised data. Similar results are obtained for PCA-S207, with a weighted average $^{207}\text{Pb}/^{206}\text{Pb}$ date of 1884.0 ± 16.0 Ma (Fig. 9c, normalised to R10, NIGL ID-TIMS data) and 1875 ± 12.0 Ma (Fig. 9d, normalised to Sugluk-4). If R10 is

normalised to Sugluk-4 (Fig. 9e), the datapoints appear non-equivalent and most are discordant on a Tera-Wasserburg diagram, with a reproducibility of the $^{207}\text{Pb}/^{206}\text{Pb}$ and $^{206}\text{Pb}/^{238}\text{U}$ ratios (mass bias corrected only) of 3.9 and 4.1 % (2σ) versus 2.7 and 2.9 % for Sugluk-4 during the same session, reflecting the presence and variability of common Pb in R10. Finally, the four Sugluk-4 grains analysed over the same session are shown in Fig. 10 normalised to R10 (using the average of NIGL ID-TIMS data from this study). All datapoints with the exception of one (that belongs to the positive tail of datapoints high in relative common Pb content in Fig. 6a) are concordant within their analytical uncertainty, and for all the individual grains the weighted average of the $^{207}\text{Pb}/^{206}\text{Pb}$ dates overlaps within uncertainty with the $^{207}\text{Pb}/^{206}\text{Pb}$ ID-TIMS date obtained for the same grain as shown in Fig. 10, although the laser ablation date is systematically older by 0.5–1.3%. This reflects both: i) the natural variation shown by the R10 ID-TIMS data (Luvizotto et al., 2009 and this study) and the difficulty in assigning absolute ratios to such a naturally heterogeneous material to be used as the reference for normalisation; and ii) any intragrain variation of Sugluk 4 (N.B. ID-TIMS values in Fig. 10 on *the same* grains as the laser ablation data).

Overall, these results show that: (1) Sugluk-4 is a rutile characterized by nearly concordant ID-TIMS and concordant (within uncertainty) LA U-Pb analyses, with long-term reproducibility on the order of 2–4 %, ~ 1% more than natural zircon materials routinely used for U-Pb dating; (2) the intra- and inter-grain scatter in the isotopic ratios of Sugluk-4 are interpreted to reflect real geological rather than analytical phenomena and are most likely caused by cooling-related diffusion compatible with the slow cooling of many natural rutiles from granulite terrains; (3) PCA-S207 is characterized by a larger variability than Sugluk-4, usually within 4% for individual grains; (4) R10 has a large degree of intergrain heterogeneity with respect to common Pb and each portion needs to be characterised for homogeneity if a common Pb correction is not to be applied to the data; (5) we recognise some real variation between and within grains likely pertaining to cooling history of many rutiles as recognised by others (e.g. Baldwin et al. 2004; Flowers et al. 2006; Kooijman et al. 2010).

Finally and most importantly for the implications to routine use as reference material, the observed total variation in $^{207}\text{Pb}/^{206}\text{Pb}$ and $^{206}\text{Pb}/^{238}\text{U}$ ratios (not corrected for common Pb) for >97% of all Sugluk-4 grains falls within the $\pm 2\%$ and $\pm 4\%$ range (at the 2σ level) generally attainable using microprobe methodologies, and it is only slightly worse for PCA-S207. Sugluk-4 and PCA-S207 therefore appear to be suitable primary and secondary reference materials for U-Pb dating of rutile by LA-ICP-MS without the requirement for correction of

common Pb. This makes these two materials similar to zircon reference materials in their ease of use and applicability and eliminates the need for an on-line common Pb correction in measuring the primary reference material which inflates the measurement uncertainties, potentially introduces systematic errors if wrong assumptions are made regarding the common Pb composition and further masks real variations in the data.

5. Detrital rutile geochronology applied to sedimentary provenance

In this section we present U-Pb data measured on detrital rutile from modern rivers draining portions of the Canadian Cordillera (British Columbia, Canada) and the Himalayas (Bhutan), in order to illustrate the applicability of detrital rutile dating and to demonstrate that young rutile can be dated successfully by LA-MC-ICP-MS. Schematic geological maps of these areas with location of sand samples are shown in Fig. 11, and the exact geographical coordinates of the samples are indicated in Table D of the Supplementary data file.

5.1 Detrital rutile samples from the Canadian Cordillera and Bhutan Himalayas

Two detrital samples are from modern rivers draining the southern Omineca belt of the Canadian Cordillera (Parrish 1995), a large area of high-grade metamorphic rocks of the core of the orogen. The belt is dissected into blocks by Eocene crustal-scale faults juxtaposing footwall rocks of high metamorphic grade against hanging wall rocks that were much cooler in the Eocene (Parrish et al., 1988; Parrish 1995, and references therein). Sample BC-04g66 is from the Columbia River in the vicinity of Revelstoke (Fig. 11a). The Columbia River in this region flows southward along the Columbia fault that bounds the Monashee Complex to the west. The latter consists of Early Proterozoic crystalline basement composed of orthogneisses and paragneisses and an unconformably overlying cover sequence, all significantly metamorphosed and deformed in latest Cretaceous-Paleogene time (Parrish 1995), with some variation in age as a function of structural level. U-Pb isotopic data from xenotime and monazite representing peak metamorphic conditions young from 64 Ma to 49 Ma with increasing structural depth within the complex (Crowley and Parrish, 1999). Anatexis of the Proterozoic basement as a result of regional prograde metamorphism is constrained by U-Pb dates from migmatitic leucosomes at 62 and 56–54 Ma (zircon) and 57 Ma (titanite), (Hinchey et al., 2006; Gervais and Brown, 2011). Sample BC-04g67 is from the Eagle River, 40 km farther west of the first sample (Fig. 11a). The Eagle River flows westward and its sediments are derived almost entirely from the erosion of the Monashee complex. Rutile U-Pb ages, reflecting cooling below ~ 500°C, are thus expected to be in the age range of ~ 50–55

Ma for detritus eroded from the Monashee complex, the primary source of rutile of these two rivers.

Four detrital rutile samples are from modern rivers draining an eastern portion of the Himalayas in Bhutan (Fig. 11b). The Himalayan orogen formed as the results of the collision between India and Asia that started at ~ 50 Ma and is still ongoing (Hodges, 2000; Najman et al., 2010 and references therein). The Himalayan tectonostratigraphic units exposed in Bhutan are separated by crustal scale southward-propagating thrust faults and from north to south are: the Tethyan sedimentary sequence (TH), a Palaeozoic-Mesozoic sedimentary succession deposited on the northern passive margin of India; the Proterozoic to early Paleozoic metasedimentary rocks and orthogneisses of the Greater Himalaya (GH), highly metamorphosed during the Tertiary with peak metamorphism being 25–17 Ma, accompanied by crustal melting and emplacement of leucogranites between 23 and 12 Ma; the Lesser Himalaya (LH), a thick succession of non metamorphic or low-grade Precambrian to Palaeozoic clastic and carbonate rocks deposited upon the northern Indian margin; the Tertiary foreland basin sediments of the Siwalik Group. Within the GH of Bhutan, klippen associated with the South Tibetan Detachment expose sedimentary rocks of greenschist facies and lower metamorphic grade (Late Proterozoic Chekha Formation). For further reading on the geology of Bhutan in order to set these samples into context the reader is referred to Gansser (1983), Grujic et al. (2002), Hollister and Grujic (2006), and McQuarrie et al. (2008). Bhutan is drained by an hydrographic system broadly N-S oriented, that cuts across the main Himalayan geological units and their tectonic boundaries and eventually empties into the Brahmaputra River in the state of Assam in India. Sample BH0108 and LB09-03 are two modern river sands from the Mo Chu and the Puna Tsang Chu (Fig. 11b). The Mo (mother) Chu (river) originates in Tibet and after joining the Pho (father) Chu by Punakha becomes the Puna Tsang Chu. The sand sample LB09-01 is from the more eastern Mangdi Chu that flows in central Bhutan, while sand LB09-02 was sampled from the Mau Khola river south of the Main Central Thrust and close to the border with India (Fig. 11b). All of these samples drain variable amounts of rock of high metamorphic grade, with some containing lesser metamorphosed metasedimentary lithologies. Detrital rutile is likely to have been derived mainly from the high grade metamorphic sources which have a predominant Tertiary Himalayan metamorphic signature.

5.2 Detrital rutile U-Pb data

LA U-Pb data of detrital rutile samples (Table D, Supplementary data file) are shown in Figs. 12 and 13 as Wetherill concordia diagrams and $^{206}\text{Pb}/^{238}\text{U}$ age probability density plots. The number of ablation spots for each sample plotted on the concordia diagrams varies from 18 to 48 as indicated, and measurement protocols were identical between samples and reference materials (Sugluk-4 and PCA-S207). For all samples, an originally larger number of grains was analysed, but some of the grains failed to produce a signal strong enough to be measured (due to low Pb and/or uranium content), especially when a smaller spot size was used (i.e., 5–10% of grains failed when a 50 μm spot size was used and up to 30% using a 35 or 40 μm spot size on fine-grained 10–15 Ma old rutile). Measured intensity of the radiogenic ^{207}Pb was low in many grains due to young age and/or low U content (Table D, Supplementary data file). These realities are reflected in Concordia diagrams by larger uncertainty ellipses and in part by arrays of data (see below).

At times two spots were ablated from the same grain to test potential age zoning and reproducibility. These always resulted in two dates overlapping within uncertainty, of which only the one determined with the lower uncertainty was eventually included in the probability plot. Typically, all samples produced a U-Pb dataset characterized by a cluster of datapoints concordant within their uncertainty with usually one array of discordant datapoints intercepting the cluster of concordant points at its lower intercept (Figs. 12 and 13). These discordant datapoints clearly reflect a higher proportion of common Pb within these analyses. To calculate a model (common Pb corrected) date for such grains each analysis is individually anchored to common Pb with a $^{207}\text{Pb}/^{206}\text{Pb}$ ratio of 0.844 ($\pm 2\%$) representing the average common Pb composition for the Mesozoic and Cenozoic time interval (251 Ma to present) calculated using the Stacey-Kramers (1975) model. Two probability density diagrams for each sample are shown in Figs. 12 and 13 that illustrate the concordant and discordant plus the projected data, with similar conclusions drawn using either. Caution should be exercised when interpreting significance of single datapoints that after projection do not overlap with a population of originally concordant datapoints. It should also be noted that this projection of data relies on the fundamental assumption that the only contribution to the offset from concordance is common Pb and assumes concordancy in the final result. However, this is likely more valid as an assumption for rutile than for zircons for example, where multiple age components are more likely to be preserved and Pb-loss is proven to occur with significant effect.

Both samples from British Columbia (BC-04g66 and BC-04g67, Fig. 12) show a ~ Paleocene-Eocene rutile age distribution (~ 42 to 77 Ma) with main clusters at ~ 52 and ~ 48 Ma for the Columbia River and the Eagle River, respectively, reflecting the documented age of the Cordilleran metamorphism that affected the source areas drained by the two rivers. The youngest detrital rutile dates at ~ 42 Ma indicate that an area of the Monashee complex was still cooling through ~ 500 °C at the time. The somewhat older few ages observed are entirely reasonable since these grains could have come from high structural levels of the Monashee Complex in which late Cretaceous metamorphic events are known, or more likely from metamorphic sources in the Selkirk Mountains to the east of the Monashee Complex, still within the drainage area of the Columbia River.

For the modern river sand samples from Bhutan (Fig. 13), the initial number of spot ablations was ~ 40–50 (using a 50 µm spot size) and 60–70 (using a 35–40 µm spot size, due to smaller sample grain size) per sample, resulting in a final average age distribution (after eliminating analyses that failed) of ~ 40 individual grains in both cases.

The Mo Chu (sample BH0108) drains the northern highest-grade part of the GH in Bhutan and shows a narrow detrital age distribution clustered around 13–15 Ma. For the downstream Puna Tsang Chu (sample LB09-03), the age range is wider (~ 10 to 26 Ma), with the main age cluster slightly older than in the Mo Chu. Narrow age clusters are shown by the Mau Khola (sample LB09-02) at ~ 13 Ma and by the Mangdi Chu (LB09-01), the easternmost of the samples, at ~ 10 Ma. We emphasize that no pre-screening e.g. based on the U content of the samples was applied, thereby more robustly representing a genuine sampling of the rutile population in the samples and avoiding bias. Although the detection limit of any instrumental set up will inevitably bias the original population towards the higher radiogenic grains, the number of grains we omitted post-analysis was smaller than if a pre-screening threshold e.g. of 5 ppm U had been applied (Zack et al., 2011). As an example, 37 spots were originally ablated for sample LB09-01, and only 2 of these rejected due to ^{207}Pb being below the detection limit, while 11 grains (30 %) with $\text{U} < 5\text{ppm}$ were successfully analysed (Table B, Supplementary data file). The results show that drainages with bedrock predominantly comprised of high grade GH rocks yield rutile U-Pb ages of 10–20 Ma. Zircons from the same samples are primarily $>480\text{ Ma}$, with only a few grains or metamorphic rims reflecting the Himalayan Miocene metamorphism (Bracciali, unpublished data). The contrast between zircon and rutile signatures is very dramatic and as such provides important complementary

information about the events within the Himalayan orogen affected by a complex polyphase history.

Acknowledgements

This work was funded by NERC grants NE/F01807X/1 to Najman and NE/F017588/1 to Parrish. We thank Craig Storey (University of Portsmouth) for the trace element data acquisition and Thomas Zack for providing fragments of R10 and R19 rutiles. The Editor Klaus Mezger and two anonymous reviewers are kindly acknowledged for their comments that allowed us to improve the manuscript.

Appendix A. Supplementary data

Supplementary data associated with this article can be found, in the online version, at doi: xxxxxxxx.

References

- Allen, C.M. and Campbell, I.H., 2007. Spot dating of detrital rutile by LA-Q-ICP-MS: a powerful provenance tool, GSA Denver Annual Meeting 28–31 October 2007, Paper no. 196–12.
- Baldwin, J.A., Bowring, S.A., Williams, M.L. and Williams, I.S., 2004. Eclogites of the Snowbird tectonic zone: petrological and U-Pb geochronological evidence for Paleoproterozoic high-pressure metamorphism in the western Canadian Shield. *Contributions to Mineralogy and Petrology* 147, 528–548.
- Birch, W.D., Barron, L.M., Magee, C. and Sutherland, F.L., 2007. Gold- and diamond-bearing White Hills Gravel, St Arnaud district, Victoria: age and provenance based on U-Pb dating of zircon and rutile. *Australian Journal of Earth Sciences* 54, 609–628.
- Black, L.P. and Gulson, B.L., 1978. The age of the Mud Tank carbonatite, Strangways Range, Northern Territory. *BMR Journal of Australian Geology and Geophysics* 3, 227–232.
- Blackburn, T., Bowring, S., Schoene, B., Mahan, K. and Dudas, F., 2011. U-Pb thermochronology: creating a temporal record of lithosphere thermal evolution. *Contributions to Mineralogy and Petrology* 162, 479–500.
- Blackburn, T.J., Bowring, S.A., Perron, J.T., Mahan, K.H., Dudas, F.O. and Barnhart, K.R., 2012. An Exhumation History of Continents over Billion-Year Time Scales. *Science* 335, 73–76.
- Carruzzo, S., Clarke, D.B., Pelrine, K.M. and MacDonald, M.A., 2006. Texture, composition, and origin of rutile in the South Mountain Batholith, Nova Scotia. *The Canadian Mineralogist* 44, 715–729.

- Cherniak, D.J., 2000. Pb diffusion in rutile. *Contributions to Mineralogy and Petrology* 139, 198-207.
- Clark, D.J., Hensen, B.J. and Kinny, P.D., 2000. Geochronological constraints for a two-stage history of the Albany-Fraser Orogen, Western Australia. *Precambrian Research* 102, 155-183.
- Corfu, F. and Andrews, A.J., 1986. A U–Pb age for mineralized Nipissing diabase, Gowganda, Ontario. *Canadian Journal of Earth Sciences* 23, 107-109.
- Corfu, F. and Muir, T.L., 1989. The Hemlo-Heron Bay greenstone belt and Hemlo Au-Mo deposit, Superior Province, Ontario, Canada 2. Timing of metamorphism, alteration and Au mineralization from titanite, rutile, and monazite U-Pb geochronology. *Chemical Geology: Isotope Geoscience section* 79, 201-223.
- Cox, R.A., Indares, A. and Dunning, G.R., 2002. Temperature-time paths in the high-P Manicouagan Imbricate zone, eastern Grenville Province: Evidence for two metamorphic events. *Precambrian Research* 117, 225-250.
- Crowley and Parrish, 1999. U–Pb isotopic constraints on diachronous metamorphism in the northern Monashee complex, southern Canadian Cordillera. *Journal of Metamorphic Geology* 17, 483-502.
- Davis, W.J., 1997. U-Pb zircon and rutile ages from granulite xenoliths in the Slave province: Evidence for mafic magmatism in the lower crust coincident with Proterozoic dike swarms. *Geology* 25, 343-346.
- Dodson, M.H., 1973. Closure temperature in cooling geochronological and petrological systems. *Contributions to Mineralogy and Petrology* 40, 259-274.
- Dodson, M.H., 1986. Closure profiles in cooling systems. *Materials Science Forum* 7, 145-154.
- Ewing, T.A., Rubatto, D., Eggins, S.M. and Hermann, J., 2011. In situ measurement of hafnium isotopes in rutile by LA-C-ICPMS: Protocol and applications. *Chemical Geology* 281, 72-82.
- Ferry, J. and Watson, E., 2007. New thermodynamic models and revised calibrations for the Ti-in-zircon and Zr-in-rutile thermometers. *Contributions to Mineralogy and Petrology* 154, 429-437.
- Flowers, R.M., Bowring, S.A., Tulloch, A.J., Klepeis, K.A., 2005. Tempo of burial and exhumation within the deep roots of a magmatic arc, Fiordland, New Zealand. *Geology* 33, 17-20.
- Flowers, R.M. et al., 2006. Multistage exhumation and juxtaposition of lower continental crust in the western Canadian Shield: Linking high-resolution U-Pb and $^{40}\text{Ar}/^{39}\text{Ar}$ thermochronometry with pressure-temperature-deformation paths. *Tectonics* 25, TC4003.
- Gansser, A., 1983. *Geology of the Bhutan Himalaya*. Birkhauser Verlag, Basel, 181 pp.

- Gerstenberger, H. and Haase, G., 1997. A highly effective emitter substance for mass spectrometric Pb isotope ratio determinations. *Chemical Geology* 136, 309-312.
- Gervais, F.I. and Brown, R.L., 2011. Testing modes of exhumation in collisional orogens: Synconvergent channel flow in the southeastern Canadian Cordillera. *Lithosphere* 3, 55-75.
- Grujic, D., Hollister, L.S. and Parrish, R.R., 2002. Himalayan metamorphic sequence as an orogenic channel: insight from Bhutan. *Earth and Planetary Science Letters* 198, 177-191.
- Hanmer, S., Parrish, R., Williams, M. and Kopf, C., 1994. Striding-Athabasca mylonite zone: Complex Archean deep-crustal deformation in the East Athabasca mylonite triangle, northern Saskatchewan. *Canadian Journal of Earth Sciences* 31, 1287-1300.
- Harrison, T.M., Trail, D., Schmitt, A.K. and Watson, E.B., 2007. Rutile ^{207}Pb - ^{206}Pb ages in the Jack Hills quartzite, Western Australia. *Geochimica et Cosmochimica Acta*, 71 (15, Supplement 1), A383.
- Hinchey, A.M., Carr, S.D., McNeill, P.D. and Rayner, N., 2006. Paleocene-Eocene high-grade metamorphism, anatexis, and deformation in the Thor-Odin dome, Monashee complex, southeastern British Columbia. *Canadian Journal of Earth Sciences* 43, 1341-1365.
- Hodges, K.V., 2000. Tectonics of the Himalaya and southern Tibet from two perspectives. *Geological Society of America Bulletin* 112, 324-350.
- Hollister, L.S. and Grujic, D., 2006. Pulsed channel flow in Bhutan. In: R.D. Law, M. Searle and L. Godin (Eds.), *Channel Flow, Extrusion and Exhumation of Lower-mid Crust in Continental Collision Zones*. Geological Society of London Special Publications, pp. 415-423.
- Horstwood, M.S.A., Foster, G.L., Parrish, R.R., Noble, S.R. and Nowell, G.M., 2003. Common-Pb corrected in situ U-Pb accessory mineral geochronology by LA-MC-ICP-MS. *Journal of Analytical Atomic Spectrometry* 18, 837-846.
- Jackson, S.E., Pearson, N.J., Griffin, W.L. and Belousova, E.A., 2004. The application of laser ablation-inductively coupled plasma-mass spectrometry to in situ U-Pb zircon geochronology. *Chemical Geology* 211, 47-69.
- Jaffey, A.H., Flynn, K.F., Glendenin, L.E., Bentley, W.C., Essling, A.M., 1971. Precision Measurement of Half-Lives and Specific Activities of ^{235}U and ^{238}U . *Physical Review C*, 4, 1889-1906.
- Kooijman, E., Mezger, K. and Berndt, J., 2010. Constraints on the U-Pb systematics of metamorphic rutile from in situ LA-ICP-MS analysis. *Earth and Planetary Science Letters* 293, 321-330.
- Kylander-Clark, A.R.C., Hacker, B.R. and Mattinson, J.M., 2008. Slow exhumation of UHP terranes: Titanite and rutile ages of the Western Gneiss Region, Norway. *Earth and Planetary Science Letters* 272, 531-540.

- Li, Q.-l., Lin, W., Su, W., Li, X.-h., Shi, Y.-h., Liu, Y. and Tang, G.-q., 2011. SIMS U-Pb rutile age of low-temperature eclogites from southwestern Chinese Tianshan, NW China. *Lithos* 122, 76-86.
- Ludwig, K. and Cooper, J., 1984. Geochronology of Precambrian granites and associated U-Ti-Th mineralization, northern Olary province, South Australia. *Contributions to Mineralogy and Petrology* 86, 298-308.
- Ludwig, K.R., 2003. Isoplot/Ex Version 3.00: A Geochronological Toolkit for Microsoft Excel. Berkeley Geochronology Center, Berkeley, CA.
- Luvizotto, G.L. et al., 2009. Rutile crystals as potential trace element and isotope mineral standards for microanalysis. *Chemical Geology* 261, 346-369.
- McQuarrie, N., Robinson, D., Long, S., Tobgay, T., Grujic, D., Gehrels, G. and Ducea, M., 2008. Preliminary stratigraphic and structural architecture of Bhutan: Implications for the along strike architecture of the Himalayan system. *Earth and Planetary Science Letters* 272, 105-117.
- Meinhold, G., Anders, B., Kostopoulos, D. and Reischmann, T., 2008. Rutile chemistry and thermometry as provenance indicator: An example from Chios Island, Greece. *Sedimentary Geology* 203, 98-111.
- Meinhold, G., 2010. Rutile and its applications in earth sciences. *Earth-Science Reviews* 102, 1-28.
- Meinhold, G., Morton, A.C., Fanning, C.M. and Whitham, A.G., 2011. U-Pb SHRIMP ages of detrital granulite-facies rutiles: further constraints on provenance of Jurassic sandstones on the Norwegian margin. *Geological Magazine* 148, 473-480.
- Meyer, M., John, T., Brandt, S.n. and Klemd, R., 2011, Trace element composition of rutile and the application of Zr-in-rutile thermometry to UHT metamorphism (Epupa Complex, NW Namibia). *Lithos* 126, 388-401.
- Mezger, K., Hanson, G.N. and Bohlen, S.R., 1989. High-precision U-Pb ages of metamorphic rutile: application to the cooling history of high-grade terranes. *Earth and Planetary Science Letters* 96, 106-118.
- Morton, A. and Chenery, S., 2009. Detrital Rutile Geochemistry and Thermometry as Guides to Provenance of Jurassic-Paleocene Sandstones of the Norwegian Sea. *Journal of Sedimentary Research* 79, 540-553.
- Najman, Y. et al., 2010. Timing of India-Asia collision: Geological, biostratigraphic, and palaeomagnetic constraints. *J. Geophys. Res.* 115, B12416.
- Okay, N., Zack, T., Okay, A.I. and Barth, M., 2011. Sinistral transport along the Trans-European Suture Zone: detrital zircon–rutile geochronology and sandstone petrography from the Carboniferous flysch of the Pontides. *Geological Magazine* 148, 380-403.
- Parrish, R.R., 1989. U-Pb geochronology of the Cape Smith Belt and Sugluk block, northern Quebec. 1989.

- Parrish, R.R., 1995. Thermal evolution of the southeastern Canadian Cordillera. *Canadian Journal of Earth Sciences* 32, 1618-1642.
- Parrish, R.R., Carr, S.D. and Parkinson, D.L., 1988. Eocene extensional tectonics and geochronology of the Southern Omineca Belt, British Columbia and Washington. *Tectonics* 7, 181-212.
- Pearce, N.J.G. et al., 1997. A Compilation of New and Published Major and Trace Element Data for NIST SRM 610 and NIST SRM 612 Glass Reference Materials. *Geostandards Newsletter* 21, 115-144.
- Rösel, D., Zack, T., Barth, M., Möller, A. and Oalman, J., 2011. U/Pb Age Spectra of Detrital Rutile as a Powerful Tool for Provenance Analysis, Goldschmidt Conference, Prague.
- Rudnick, R.L., Barth, M., Horn, I., McDonough, W.F., 2000. Rutile-Bearing Refractory Eclogites: Missing Link Between Continents and Depleted Mantle. *Science* 287, 278-281.
- Schärer, U., Krogh, T.E. and Gower, C.F., 1986. Age and evolution of the Grenville Province in eastern Labrador from U-Pb systematics in accessory minerals. *Contributions to Mineralogy and Petrology* 94, 438-451.
- Schmitt, A.K., Zack, T., 2012. High-sensitivity U–Pb rutile dating by secondary ion mass spectrometry (SIMS) with an O₂⁺ primary beam. *Chemical Geology* 332–333, 65-73.
- Schmitz, M. and Bowring, S., 2003. Constraints on the thermal evolution of continental lithosphere from U-Pb accessory mineral thermochronometry of lower crustal xenoliths, southern Africa. *Contributions to Mineralogy and Petrology* 144, 592-618.
- Schmitz, M.D. and Schoene, B., 2007. Derivation of isotope ratios, errors, and error correlations for U-Pb geochronology using ²⁰⁵Pb-²³⁵U-(²³³U)-spiked isotope dilution thermal ionization mass spectrometric data. *Geochem. Geophys. Geosyst.* 8, Q08006.
- Sircombe, K., 1995. SHRIMP ion probe provenance studies of heavy detrital minerals in coastal sands and sedimentary rocks of east Australia. *Third Australian Conference on Geochronology and Isotope Geoscience, Abstracts*, 32.
- Sláma, J. et al., 2008. Plešovice zircon - A new natural reference material for U-Pb and Hf isotopic microanalysis. *Chemical Geology* 249, 1-35.
- Stacey, J.S. and Kramers, J.D., 1975. Approximation of terrestrial lead isotope evolution by a two-stage model. *Earth and Planetary Science Letters* 26, 207-221.
- Storey, C.D., Smith, M.P. and Jeffries, T.E., 2007. In situ LA-ICP-MS U-Pb dating of metavolcanics of Norrbotten, Sweden: Records of extended geological histories in complex titanite grains. *Chemical Geology* 240, 163-181.
- Taylor, R., Clark, C., Reddy, S.M., 2012. The effect of grain orientation on secondary ion mass spectrometry (SIMS) analysis of rutile. *Chemical Geology* 300–301, 81-87.

- Thomas, R.J. et al., 2010. The Mecubúri and Alto Benfica Groups, NE Mozambique: Aids to unravelling ca. 1 and 0.5 Ga events in the East African Orogen. *Precambrian Research* 178, 72-90.
- Tomkins, H.S., Powell, R. and Ellis, D.J., 2007. The pressure dependence of the zirconium-in-rutile thermometer. *Journal of Metamorphic Geology* 25, 703-713.
- Treloar, P.J., O'Brien, P.J., Parrish, R.R. and Khan, M.A., 2003. Exhumation of early Tertiary, coesite-bearing eclogites from the Pakistan Himalaya. *Journal of the Geological Society* 160, 367-376.
- Triebold, S., von Eynatten, H., Luvizotto, G.L. and Zack, T., 2007. Deducing source rock lithology from detrital rutile geochemistry: An example from the Erzgebirge, Germany. *Chemical Geology* 244, 421-436.
- Vry, J.K. and Baker, J.A., 2006. LA-MC-ICPMS Pb-Pb dating of rutile from slowly cooled granulites: Confirmation of the high closure temperature for Pb diffusion in rutile. *Geochimica et Cosmochimica Acta* 70, 1807-1820.
- Watson, E., Wark, D. and Thomas, J., 2006. Crystallization thermometers for zircon and rutile. *Contributions to Mineralogy and Petrology* 151, 413-433.
- Wiedenbeck, M. et al., 1995. Three natural zircon standards for U-Th-Pb, Lu-Hf, trace element and REE analyses. *Geostandards Newsletter* 19, 1-23.
- Zack, T., von Eynatten, H. and Kronz, A., 2004a. Rutile geochemistry and its potential use in quantitative provenance studies. *Sedimentary Geology* 171, 37-58.
- Zack, T., Moraes, R. and Kronz, A., 2004b. Temperature dependence of Zr in rutile: empirical calibration of a rutile thermometer. *Contributions to Mineralogy and Petrology* 148, 471-488.
- Zack, T., Stockli, D., Luvizotto, G., Barth, M., Belousova, E., Wolfe, M. and Hinton, R., 2011. In situ U-Pb rutile dating by LA-ICP-MS: ^{208}Pb correction and prospects for geological applications. *Contributions to Mineralogy and Petrology* 162, 515-530.

Table 1

Trace element composition of rutile (ppm; LA-quad-ICP-MS data).

	Al	Sc	V	Cr	Zr	Nb	Mo	Sn	Hf	Ta	W	U	Pb	Zr/Hf	Nb/Ta	Cr/Nb
measured mass	27	45	51	52	90	93	95	118	177	181	182	238	(b)	-	-	-
(a)	20	8	5	4	6	4	8	7	7	9	21	7	10	9	10	6
<i>Sugluk-4, granulite facies quartzite, Sugluk group, 62° 16.9' N, 75° 37.3' W</i>																
r500_a	57	24	2010	1140	783	1550	65	30	49	176	226	95	-	16	9	0.74
r500_b	76	24	2090	1200	882	1600	73	33	55	177	230	96	-	16	9	0.75
r500_c	39	24	2090	1130	869	1630	66	32	56	162	214	96	-	16	10	0.69
r500_d	39	25	2010	1100	821	1530	73	33	52	164	223	96	-	16	9	0.72
r500_f	66	24	2150	1140	658	1620	71	35	42	174	237	98	-	16	9	0.70
r6_A	29	4.9	2930	798	666	1150	67	28	36	19	5	24	10	19	62	0.69
r6_B	65	5.3	3230	804	699	1240	59	30	41	40	11	25	10	17	31	0.65
r6_C	42	5.5	3030	813	676	1300	63	31	41	57	14	24	10	16	23	0.63
r6_D	30	5.2	3070	788	602	1300	71	30	37	63	18	24	10	16	21	0.61
r7_A	89	14	1700	940	686	1760	41	30	43	151	207	81	33	16	12	0.53
r7_B	67	16	1730	899	710	1690	41	30	43	132	184	78	32	17	13	0.53
r7_C	60	12	1680	941	797	1690	40	29	49	124	182	79	32	16	14	0.56
r7_D	31	19	1760	965	832	1690	42	30	49	117	164	78	32	17	14	0.57
r11_A	48	3.4	1880	666	882	1140	36	26	59	25	5	27	11	15	47	0.58
r11_B	44	3.5	1950	629	919	1340	38	31	58	31	6	27	11	16	43	0.47
r11_C	58	4.1	1950	590	842	1250	41	26	54	42	6	25	10	16	30	0.47
r13_A	20	5.8	2580	715	730	1250	47	28	44	82	10	25	9	17	15	0.57
r13_B	27	4.9	2490	713	721	1190	48	27	45	76	10	25	10	16	16	0.60
r13_C	42	4.9	2600	711	732	1300	51	28	44	82	11	26	10	17	16	0.55
r18_A	7	3.0	5980	1450	1020	1540	33	37	66	123	762	81	-	16	13	0.94
r18_B	12	3.0	5690	1410	1020	1480	33	33	66	125	774	82	-	16	12	0.95
r18_C	13	3.6	6150	1410	1030	1490	35	37	65	126	765	80	-	16	12	0.95
r18_D	13	3.2	5720	1400	1060	1530	32	34	67	128	789	78	-	16	12	0.92
r18_E	5	3.5	5570	1420	941	1490	37	35	60	140	803	80	-	16	11	0.95
r502_A	35	12	2460	840	657	1850	46	30	44	123	153	80	-	15	15	0.45
r502_B	43	11	2590	804	694	1740	46	30	48	149	178	78	-	14	12	0.46
r504_A	75	5.8	2960	869	1230	1260	47	31	60	63	5	29	-	20	20	0.69
r504_B	28	5.3	3190	916	1260	1300	50	32	63	75	5	29	-	20	17	0.70
<i>PCA-S207, granulite facies garnet-bearing paragneiss, East Atabasca Mylonite triangle, 59° 21.6' N, 106° 1.7' W</i>																
r500_a	78	1.3	4890	1340	770	762	14	5.6	21	10	5	39	-	37	75	1.76
r500_b	73	1.5	4700	1290	799	766	15	5.0	23	14	8	38	-	35	56	1.68
r500_c	59	1.4	4750	1360	819	785	14	5.6	26	16	10	39	-	32	48	1.73
r500_d	49	1.7	4740	1370	847	789	14	5.7	26	20	14	38	-	33	40	1.74
r500_e	53	1.4	4890	1310	825	788	14	5.5	26	19	16	40	-	32	41	1.66
r500_f	111	1.4	4800	1340	823	785	15	5.0	25	15	10	40	-	33	51	1.71
r500_g	128	1.2	4580	1310	813	789	12	5.5	25	15	10	40	-	32	52	1.66
r500_h	68	1.4	4850	1300	801	752	13	5.0	24	14	8	37	-	34	53	1.73
r7_A	92	1.6	2760	961	1300	1930	44	8.1	57	69	29	17	7	23	28	0.50
r7_B	98	1.8	2780	983	1350	1960	42	7.3	60	87	39	18	7	23	22	0.50
r7_C	88	2.1	2790	887	1320	1960	38	7.4	60	123	49	17	7	22	16	0.45
r7_D	85	2.6	2850	919	1260	1960	23	9.1	57	130	54	18	7	22	15	0.47
r7_E	88	1.7	2720	899	1150	1870	42	7.7	39	24	3	17	7	29	78	0.48
r7_F	94	1.9	2680	893	1260	1900	41	7.8	49	47	15	17	7	26	41	0.47
r7_G	101	1.8	2740	915	1380	1930	40	8.1	58	73	33	18	7	24	26	0.47
r8_A	65	1.7	4030	1350	542	1510	28	4.9	22	33	5	18	9	24	46	0.89
r8_B	42	2.1	3950	1390	577	1420	25	3.5	25	31	11	20	10	24	46	0.98
r8_C	41	2.2	4100	1520	704	1450	27	3.8	31	38	19	23	10	23	39	1.05
r8_D	36	1.9	4100	1400	911	1650	27	4.2	41	75	20	23	10	22	22	0.85
r8_F	36	1.7	3920	1420	758	1590	27	4.5	36	70	21	18	8	21	23	0.89
r9_A	74	1.1	4360	1460	1180	1390	22	8.4	47	80	27	23	9	25	17	1.05
r9_B	69	1.4	4390	1590	1150	1430	22	7.7	46	82	29	23	9	25	17	1.11
r10_A	53	1.6	4790	876	663	569	12	6.9	23	30	7	20	9	29	19	1.54
r10_B	124	1.7	4800	863	627	561	10	6.7	20	20	4	19	8	32	28	1.54
r10_C	55	2.3	4690	818	645	584	12	6.7	20	16	4	19	8	32	37	1.40
r11_A	49	1.4	4390	1440	1210	1310	58	5.6	42	80	37	15	6	29	16	1.10
r11_B	180	1.4	4830	1490	1360	1280	52	7.0	49	55	24	15	6	28	23	1.16
r11_C	82	1.1	4610	1480	1390	1200	59	6.6	51	38	11	15	6	27	32	1.23
r501_A	66	1.2	4240	1420	1000	1790	49	8.1	36	40	7	14	-	28	45	0.79
r501_B	46	2.4	4410	1040	945	1600	20	6.7	31	29	7	15	-	30	55	0.65
r503_A	76	1.5	5420	1690	1040	1540	37	4.8	49	66	24	19	-	21	23	1.10
r503_B	69	1.4	5390	1740	1090	1570	30	3.8	50	81	32	20	-	22	19	1.11
r504_A	59	1.2	4310	1190	955	431	20	4.8	31	12	7	12	-	31	37	2.76
r504_B	55	1.2	4530	1250	970	433	18	5.0	30	13	8	12	-	33	35	2.89

(a) external reproducibility (1SD)

(b) Pb = ²⁰⁶Pb + ²⁰⁷Pb as measured by LA-MC-ICP-MS, ignoring ²⁰⁴Pb and ²⁰⁸Pb (the latter b.d.l. of LA-quad-ICP-MS) which together are much less than 1% of total Pb

Table 2

T as a function of Zr-in-rutile at P=6kbar

<i>Sugluk-4</i>	T (°C) ^(a)	<i>PCA-S2</i>	T (°C) ^(a)
<i>r6_D</i>	688	<i>r8_A</i>	679
<i>r502_A</i>	696	<i>r8_B</i>	685
<i>r500_f</i>	696	<i>r10_B</i>	692
<i>r6_A</i>	697	<i>r10_C</i>	695
<i>r6_C</i>	699	<i>r10_A</i>	697
<i>r7_A</i>	700	<i>r8_C</i>	702
<i>r502_B</i>	701	<i>r8_F</i>	709
<i>r6_B</i>	702	<i>r500_a</i>	710
<i>r7_B</i>	703	<i>r500_b</i>	714
<i>r13_B</i>	704	<i>r500_h</i>	714
<i>r13_A</i>	706	<i>r500_g</i>	715
<i>r13_C</i>	706	<i>r500_c</i>	716
<i>r500_a</i>	712	<i>r500_f</i>	716
<i>r7_C</i>	713	<i>r500_e</i>	717
<i>r500_d</i>	716	<i>r500_d</i>	719
<i>r7_D</i>	717	<i>r8_D</i>	726
<i>r11_C</i>	719	<i>r501_B</i>	729
<i>r500_c</i>	721	<i>r504_A</i>	730
<i>r500_b</i>	723	<i>r504_B</i>	732
<i>r11_A</i>	723	<i>r501_A</i>	735
<i>r11_B</i>	727	<i>r503_A</i>	738
<i>r18_E</i>	729	<i>r503_B</i>	743
<i>r18_A</i>	737	<i>r7_E</i>	748
<i>r18_B</i>	737	<i>r9_B</i>	748
<i>r18_C</i>	737	<i>r9_A</i>	751
<i>r18_D</i>	740	<i>r11_A</i>	753
<i>r504_A</i>	755	<i>r7_D</i>	757
<i>r504_B</i>	757	<i>r7_F</i>	757
		<i>r7_A</i>	760
		<i>r7_C</i>	762
		<i>r7_B</i>	764
		<i>r11_B</i>	765
		<i>r7_G</i>	766
		<i>r11_C</i>	767

(a) (based on the calibration of Tomkins et al., 2007); T at P=10 kbar is ~20°C higher than at 6 kbar

Table 3
ID-TIMS U-Th-Pb isotopic data.

(a)	Radiogenic Isotope Ratios													Isotopic Ages					Sample (Radiogenic + Initial Pb) Isotope Ratios								
	Th	²⁰⁶ Pb*	mol %	Pb*	Pb _c	²⁰⁶ Pb	²⁰⁸ Pb	²⁰⁷ Pb	²⁰⁷ Pb	²⁰⁷ Pb	²⁰⁶ Pb	corr. coef.	²⁰⁷ Pb	²⁰⁷ Pb	²⁰⁶ Pb	²³⁸ U	²⁰⁷ Pb	²⁰⁴ Pb	corr. coef.								
	U	x10 ⁻¹³ mol	²⁰⁶ Pb*	Pb _c	(pg)	²⁰⁴ Pb	²⁰⁶ Pb	²⁰⁶ Pb	% err	²³⁵ U	% err	²³⁸ U	% err	²⁰⁷ Pb/ ²³⁸ U - ²⁰⁶ Pb/ ²³⁸ U	±	²³⁵ U	±	²³⁸ U	±	²⁰⁶ Pb	% err	²⁰⁶ Pb	% err	²⁰⁴ Pb	% err	²³⁸ U/ ²⁰⁶ Pb - ²⁰⁷ Pb/ ²⁰⁶ Pb	
<i>Sugluk-4</i>																											
rT1	0.00	184.0	99.83	149	28.1	9229	0.00	0.10531	0.087	4.4437	0.18	0.30603	0.11	0.94	1719.7	1.6	1720.5	1.5	1721.2	1.6	3.2625	0.11	0.10669	0.095	0.000101	3.6	-0.67
rT2	1.99	50.0	99.93	563	3.1	23825	0.58	0.10551	0.063	4.4680	0.16	0.30712	0.09	0.95	1723.2	1.2	1725.0	1.3	1726.6	1.4	3.2552	0.09	0.10572	0.19	0.000016	84.1	-0.59
rT3	0.00	17.3	99.77	118	3.3	7647	0.00	0.10543	0.099	4.4076	0.18	0.30321	0.09	0.93	1721.7	1.8	1713.8	1.5	1707.3	1.4	3.2952	0.11	0.10618	0.50	0.000055	69.6	-0.73
rT4	0.02	1.9	96.11	7	6.5	425	0.00	0.10518	0.24	4.2744	0.35	0.29474	0.16	0.82	1717.4	4.4	1688.5	2.9	1665.2	2.3	3.3025	0.65	0.12832	3.6	0.001693	19.7	-0.99
rT5	0.00	7.4	99.57	63	2.7	4132	0.00	0.10471	0.10	4.3388	0.18	0.30052	0.09	0.95	1709.2	1.9	1700.8	1.5	1694.0	1.4	3.3242	0.19	0.10560	1.2	0.000065	137.0	-0.91
rT6	0.00	52.2	99.71	90	13.2	5607	0.00	0.10531	0.098	4.4652	0.22	0.30753	0.16	0.92	1719.6	1.8	1724.5	1.8	1728.6	2.4	3.2439	0.16	0.10740	0.19	0.000153	8.7	-0.35
rT7	0.01	31.8	99.15	30	24.1	1871	0.00	0.10540	0.10	4.4288	0.20	0.30476	0.11	0.93	1721.2	1.8	1717.7	1.6	1714.9	1.7	3.2558	0.12	0.11214	0.27	0.000494	4.2	-0.50
rT8	0.00	23.3	99.86	196	2.71	12791	0.00	0.10557	0.085	4.4499	0.18	0.30572	0.10	0.95	1724.1	1.6	1721.7	1.5	1719.7	1.6	3.2699	0.12	0.10586	0.38	0.000022	129.9	-0.58
rT9	0.00	16.8	99.72	95	4.01	6105	0.00	0.10578	0.092	4.4558	0.17	0.30552	0.091	0.95	1727.7	1.7	1722.8	1.4	1718.7	1.4	3.2687	0.12	0.10694	0.51	0.000086	45.7	-0.73
rT10	0.00	10.9	99.63	73	3.39	4716	0.00	0.10556	0.091	4.4281	0.18	0.30425	0.089	0.97	1724.0	1.7	1717.6	1.5	1712.4	1.3	3.2821	0.14	0.10681	0.79	0.000092	66.0	-0.84
<i>PCA-S207</i>																											
rT1	0.00	6.1	97.56	10	13.6	651	0.00	0.11452	0.15	5.2120	0.23	0.33009	0.11	0.86	1872.2	2.6	1854.6	1.9	1838.9	1.7	2.9612	0.14	0.13389	0.53	0.001433	3.6	-0.79
rT2	0.00	4.1	99.22	34	2.83	2115	0.00	0.11393	0.097	5.1248	0.19	0.32624	0.10	0.95	1862.9	1.8	1840.2	1.6	1820.2	1.6	3.0500	0.18	0.11818	0.91	0.000315	25.2	-0.87
rT3	0.00	26.6	97.18	9	68.6	558	0.00	0.11389	0.16	5.2076	0.23	0.33164	0.10	0.83	1862.2	2.8	1853.9	2.0	1846.4	1.7	2.9314	0.09	0.13781	0.14	0.001769	0.7	-0.69
rT4	0.08	5.0	82.33	1	95.1	89	0.02	0.11405	0.78	5.2417	0.82	0.33333	0.38	0.31	1864.8	14.2	1859.4	7.0	1854.6	6.1	2.4748	0.16	0.26462	0.24	0.01114	0.5	-0.74
<i>R10</i>																											
r1	0.00	36.5	99.59	63	12.9	4122	0.00	0.075818	0.093	1.9136	0.17	0.18306	0.085	0.98	1090.1	1.9	1085.8	1.2	1083.73	0.85	5.4421	0.09	0.079011	0.18	0.000225	4.0	-0.58
r2	0.00	95.4	99.94	415	5.1	27415	0.00	0.075800	0.10	1.9133	0.20	0.18307	0.13	0.89	1089.6	2.0	1085.7	1.3	1083.8	1.3	5.4598	0.13	0.076221	0.061	0.000030	11.7	-0.90
r3	0.01	22.3	99.70	86	5.8	5677	0.00	0.075726	0.089	1.9086	0.17	0.18279	0.086	0.98	1087.6	1.8	1084.1	1.1	1082.31	0.86	5.4571	0.09	0.077813	0.28	0.000147	10.0	-0.54
r4	0.00	125.8	99.91	276	10.1	18148	0.00	0.075801	0.084	1.9179	0.17	0.18350	0.095	0.96	1089.6	1.7	1087.3	1.1	1086.17	0.95	5.4449	0.09	0.076510	0.095	0.000050	5.2	-0.74

(a) fractions composed of single rutile grains or fragments.

(b) Model Th/U ratio calculated from radiogenic ²⁰⁸Pb/²⁰⁶Pb ratio and ²⁰⁷Pb/²³⁵U age. 0.00 indicates that Th-derived ²⁰⁸Pb was below detection limit after blank and spike subtraction.

(c) Pb* and Pb_c represent radiogenic and common Pb, respectively; mol % ²⁰⁶Pb* with respect to radiogenic, blank and initial common Pb.

(d) Measured ratio corrected for spike and fractionation only. SEM analyses, based on analysis of NBS-981 and NBS-982.

(e) Corrected for fractionation, spike, and common Pb; up to 1 pg of common Pb was assumed to be procedural blank: ²⁰⁶Pb/²⁰⁴Pb = 18.60 ± 0.80%; ²⁰⁷Pb/²⁰⁴Pb = 15.69 ± 0.32%; ²⁰⁸Pb/²⁰⁴Pb = 38.51 ± 0.74% (all uncertainties 1σ). Excess over blank was assigned to initial common Pb.

(f) Errors are 2σ, propagated using the algorithms of Schmitz and Schoene (2007).

(g) Calculations are based on the decay constants of Jaffey et al. (1971).

(h) Corrected for fractionation, spike, and blank Pb only.

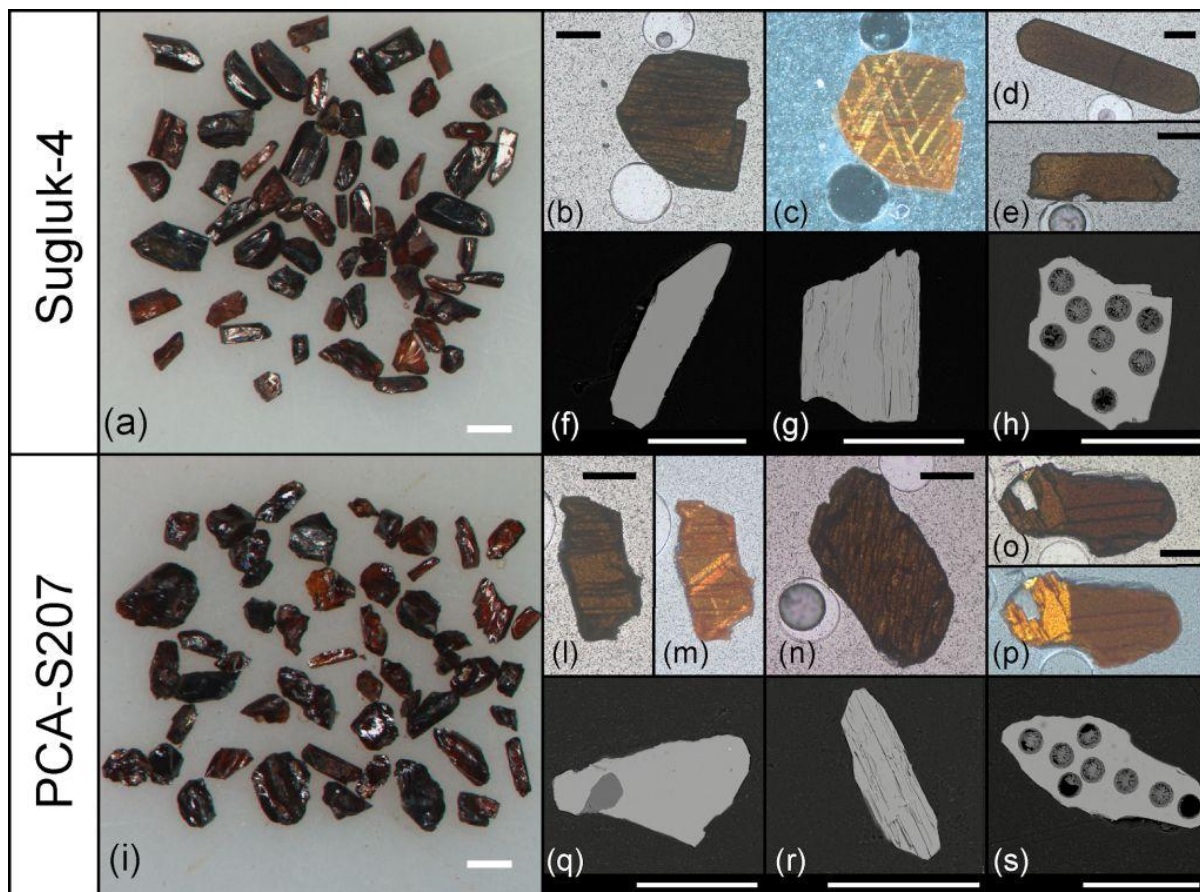


Fig. 1. Images of Sugluk-4 (a to h) and PCA-S207 (i to s) rutile grains. In all images white scale bars are 200 μm , black scale bars are 100 μm . Optical microphotographs (b), (d), (e), (l), (n), (o): plane polarised light; (c), (m), (p): crossed polarised light. (f) to (h) and (q) to (s): BSE images of polished grains; note the darker inclusion in (q) and the ablation pits in (h) and (s) after the measurement of the chemical composition by LA-ICP-MS.

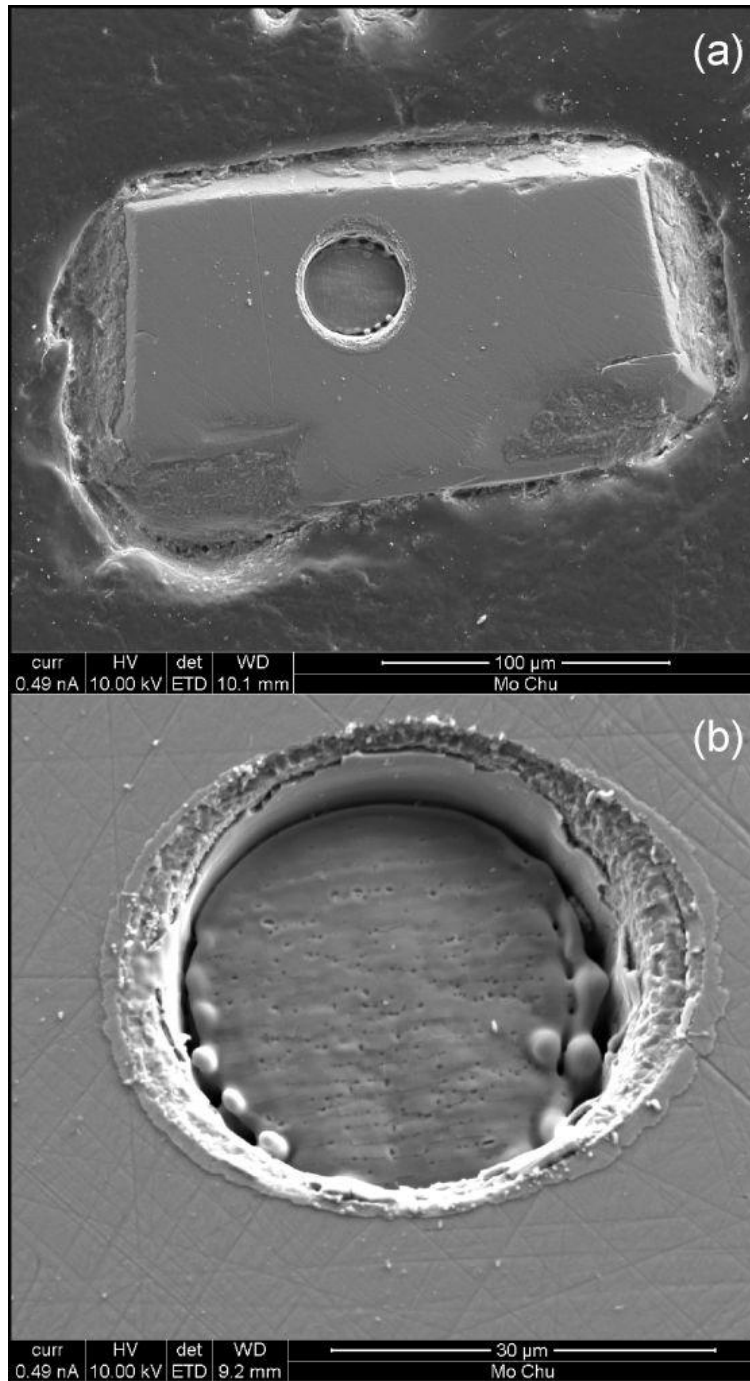


Fig. 2. (a) Secondary electron image of a rutile grain after laser ablation; (b) close up of the ablation pit (diameter 35 μm , depth 20 μm ; grain tilted on the horizontal plane by 20°).

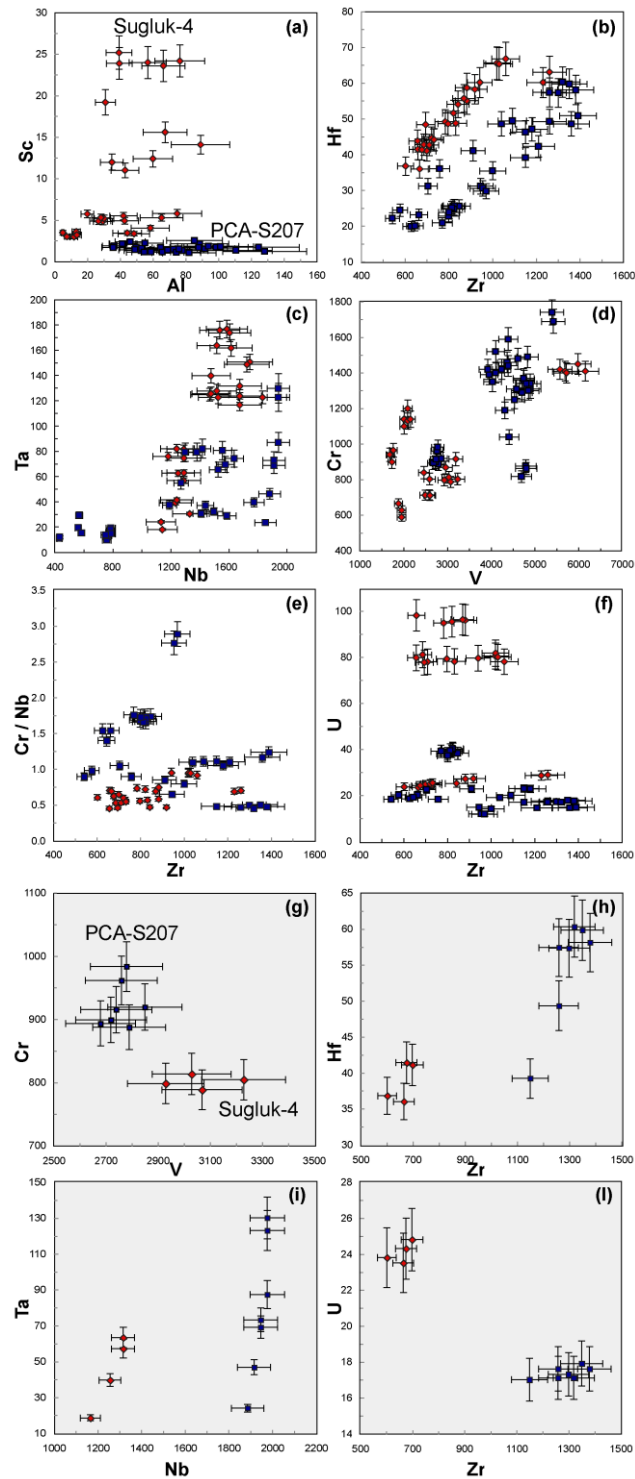


Fig. 3. Trace element composition of Sugluk-4 and PCA-S207 rutile grains determined by LA-quadrupole-ICP-MS. (a) to (f) show the chemical composition of all analysed PCA-S207 (squares) and Sugluk-4 grains (diamonds); (g) to (l) are examples of intragrain composition for PCA-S207 (grain r7, squares) and Sugluk-4 (grain r6, diamonds). All element concentrations are in ppm. Error bars represent the analytical uncertainty % (1RSD) of each element as indicated in Table 1.

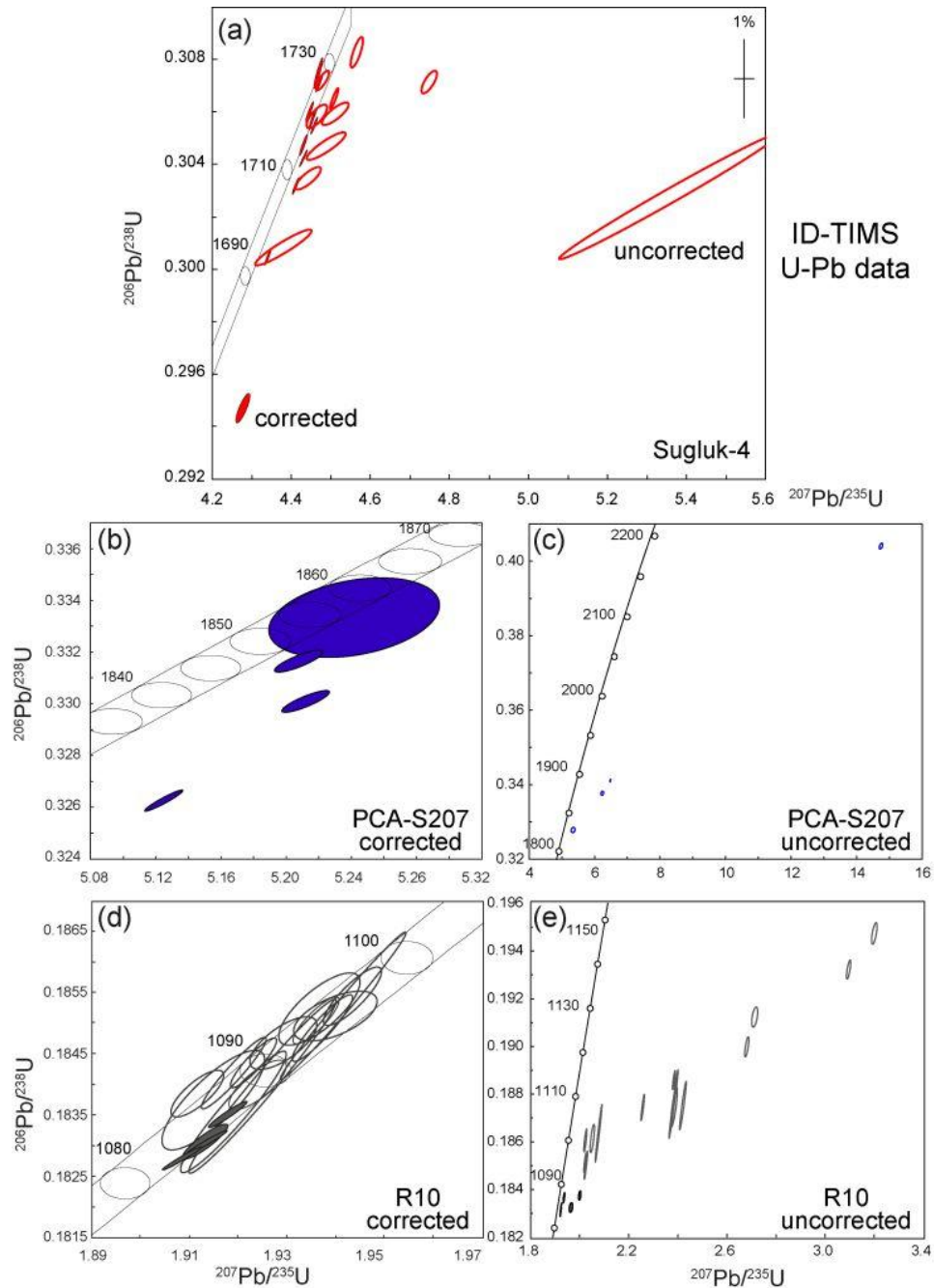


Fig. 4. Wetherill concordia diagrams of Sugluk-4, PCA-S207 and R10 rutile (U-Pb ID-TIMS data). (a) Sugluk-4 U-Pb data corrected (filled ellipses) and uncorrected for common Pb (open ellipses); PCA-S207 U-Pb data corrected (b) and uncorrected (c) for common Pb; R10 U-Pb data corrected (d) and uncorrected (e) for common Pb. In (d) and (e) data from this work (filled ellipses) are plotted along with the published data (open ellipses) of Luvizotto et al. (2009). The uncorrected ratios in (e) (open ellipses) are calculated from the published radiogenic data of Luvizotto et al., 2009 (see text for details and Table B, supplementary data file).

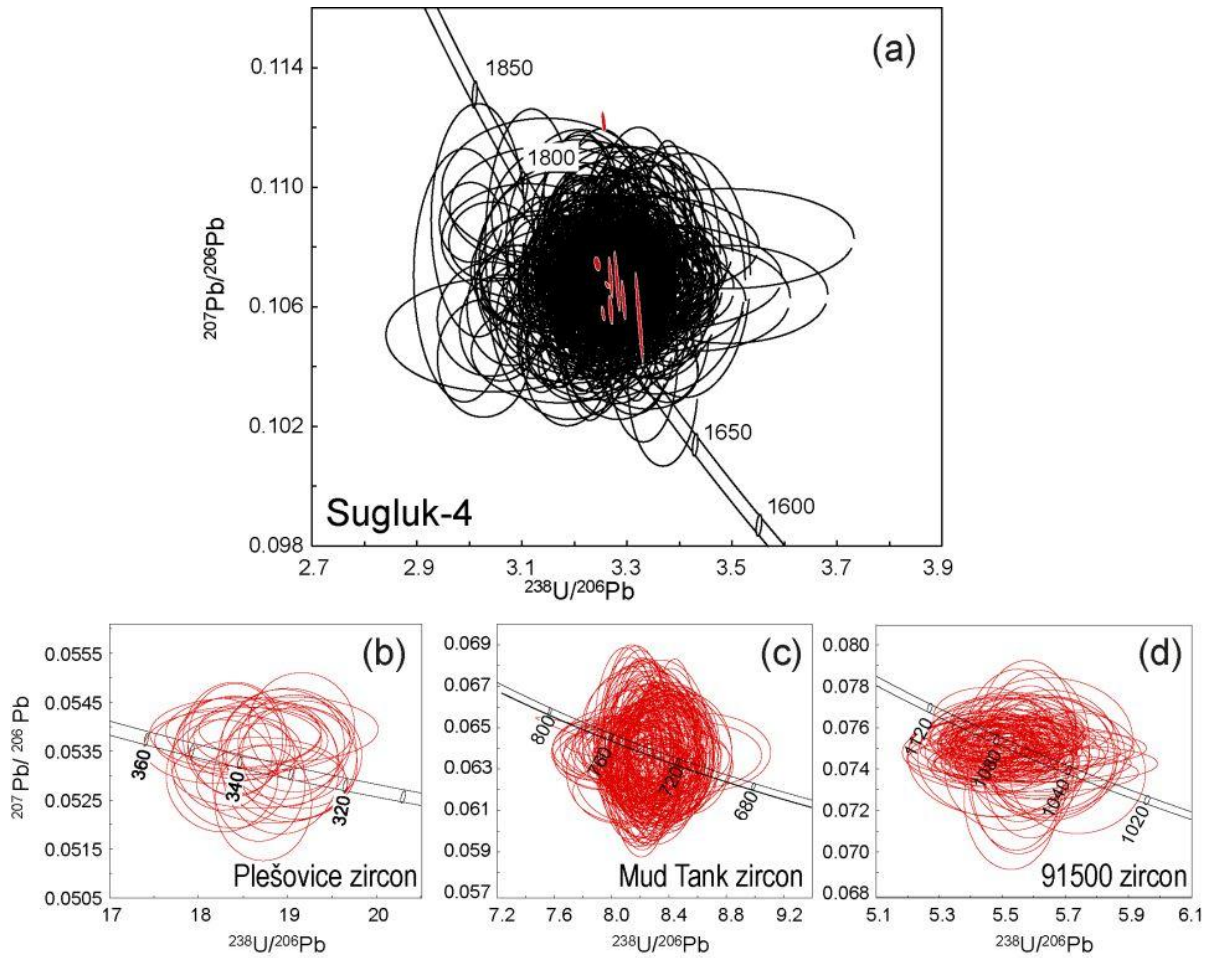


Fig. 5. Tera-Wasserburg diagrams of rutile and zircon reference materials. (a) Sugluk-4 rutile, LA U-Pb data (486 single ablation spots, open ellipses, data acquired over a period of ca. two years) and ID-TIMS data (individual grains, filled ellipses) uncorrected for common Pb. LA U-Pb Sugluk-4 data are self-normalised; the uncertainty component related to the normalization factor is not propagated into the individual $^{238}\text{Pb}/^{206}\text{U}$ data point uncertainty. (b), (c), (d) show the zircon secondary reference materials (Plešovice, Mud Tank and 91500 normalised to GJ1) analysed along with rutile over the same period.

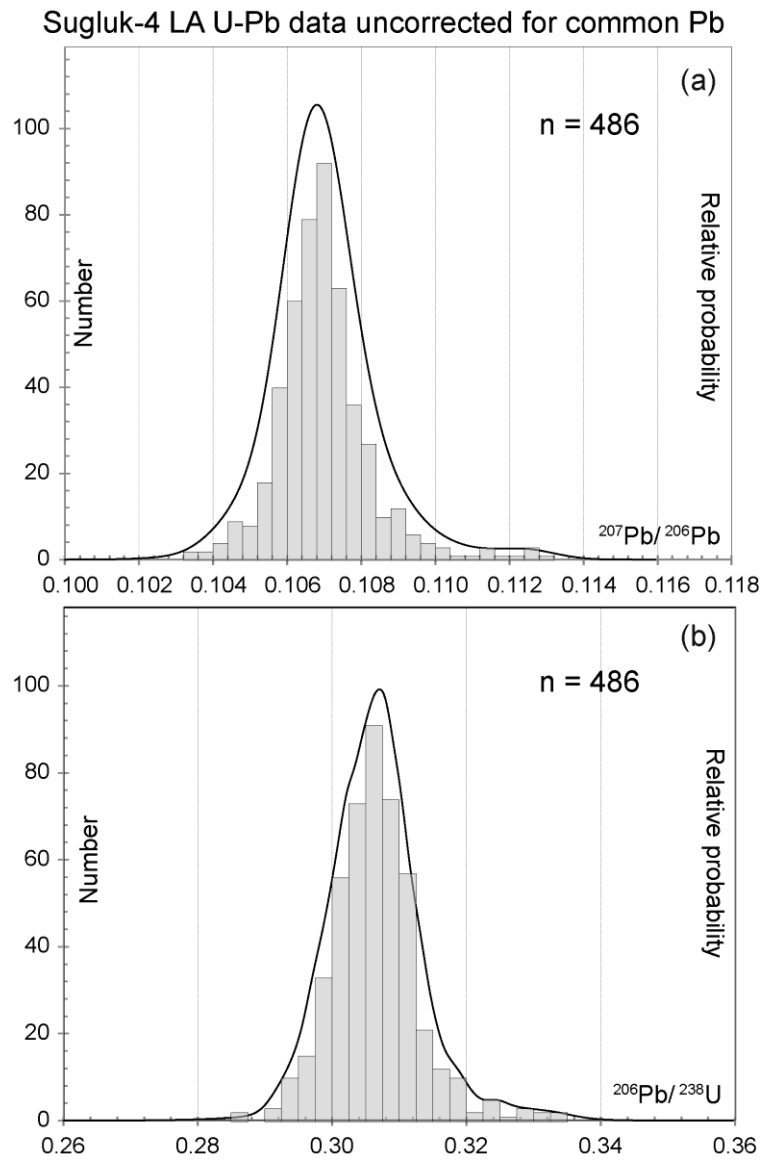


Fig. 6. Probability density plots of Sugluk-4 rutile. (a) $^{207}\text{Pb}/^{206}\text{Pb}$ and (b) $^{206}\text{Pb}/^{238}\text{U}$ ratios, same LA U-Pb data as in Fig. 5a ($n = 486$, uncorrected for common Pb).

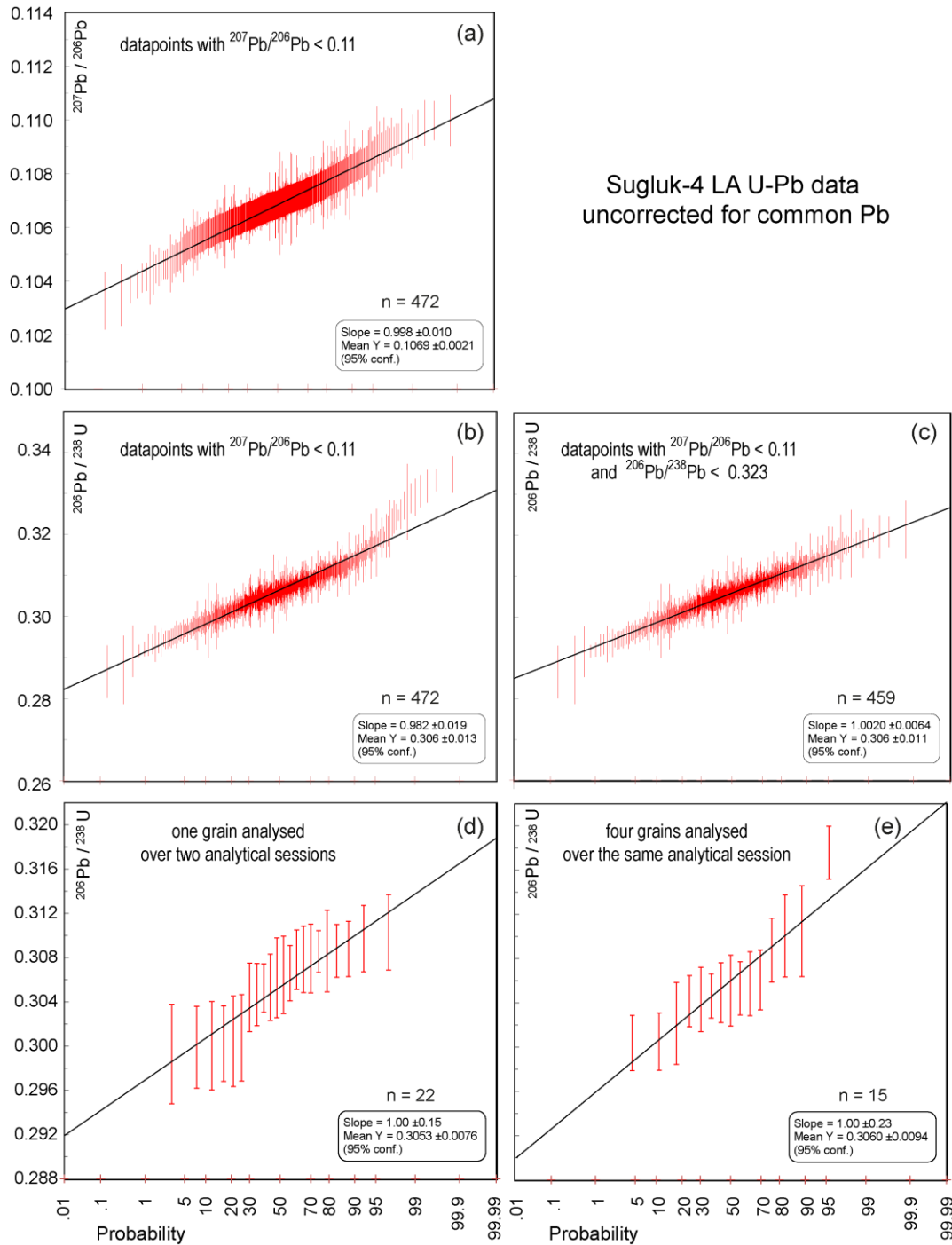


Fig. 7. Linearised probability plots of rutile Sugluk-4. (a) and (b) represent the $^{207}\text{Pb}/^{206}\text{Pb}$ and $^{206}\text{Pb}/^{238}\text{U}$ (b) ratios of 472 datapoints, same data as in Fig. 6 less 14 datapoints with $^{207}\text{Pb}/^{206}\text{Pb} > 0.11$; (c) represents the same data as in (b), less 13 datapoints with $^{206}\text{Pb}/^{238}\text{U} > 0.323$ ($n = 459$); (d) shows the $^{206}\text{Pb}/^{238}\text{U}$ ratios of one grain (r353) analysed over two different analytical sessions (22 spot ablations); (e) shows the $^{206}\text{Pb}/^{238}\text{U}$ ratios of four grains (r301, r302, r303, r304) analysed over the same session (15 spot ablations). In all diagrams data point error symbols are 1σ .

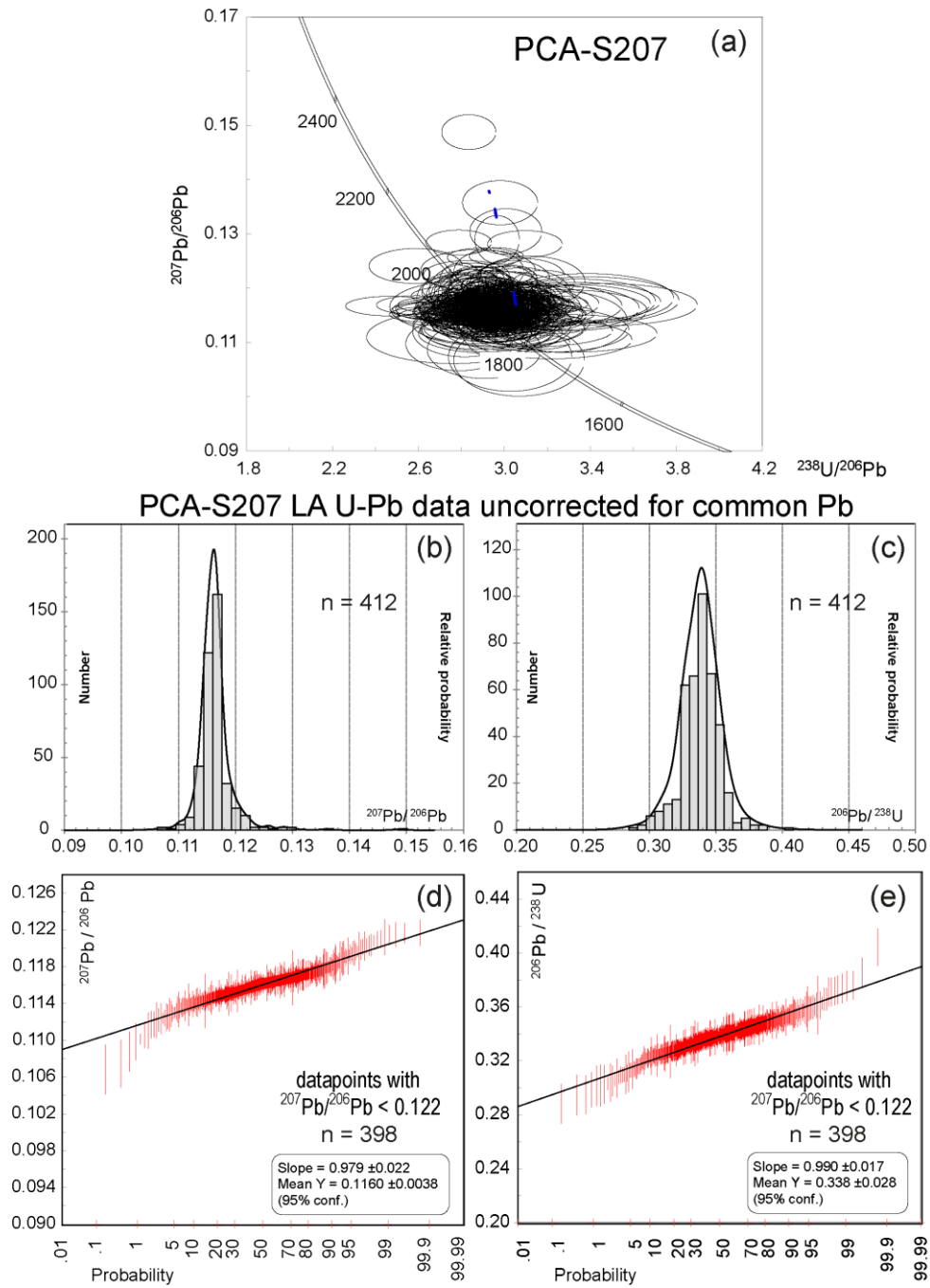


Fig. 8. PCA-S207 U-Pb data. (a) LA U-Pb data normalised to Sugluk-4 plotted as Tera-Wasserburg diagram (412 single spot ablations, open ellipses) and ID-TIMS data (individual grains, filled ellipses) uncorrected for common Pb; $^{207}\text{Pb}/^{206}\text{Pb}$ ratios (b) and $^{206}\text{Pb}/^{238}\text{U}$ (c) ratios plotted as probability density plot, same LA U-Pb data as in (a); (d) and (e) show the $^{207}\text{Pb}/^{206}\text{Pb}$ and $^{206}\text{Pb}/^{238}\text{U}$ ratios as linearised probability plots after the exclusion of 14 datapoints with $^{207}\text{Pb}/^{206}\text{Pb} > 0.122$.

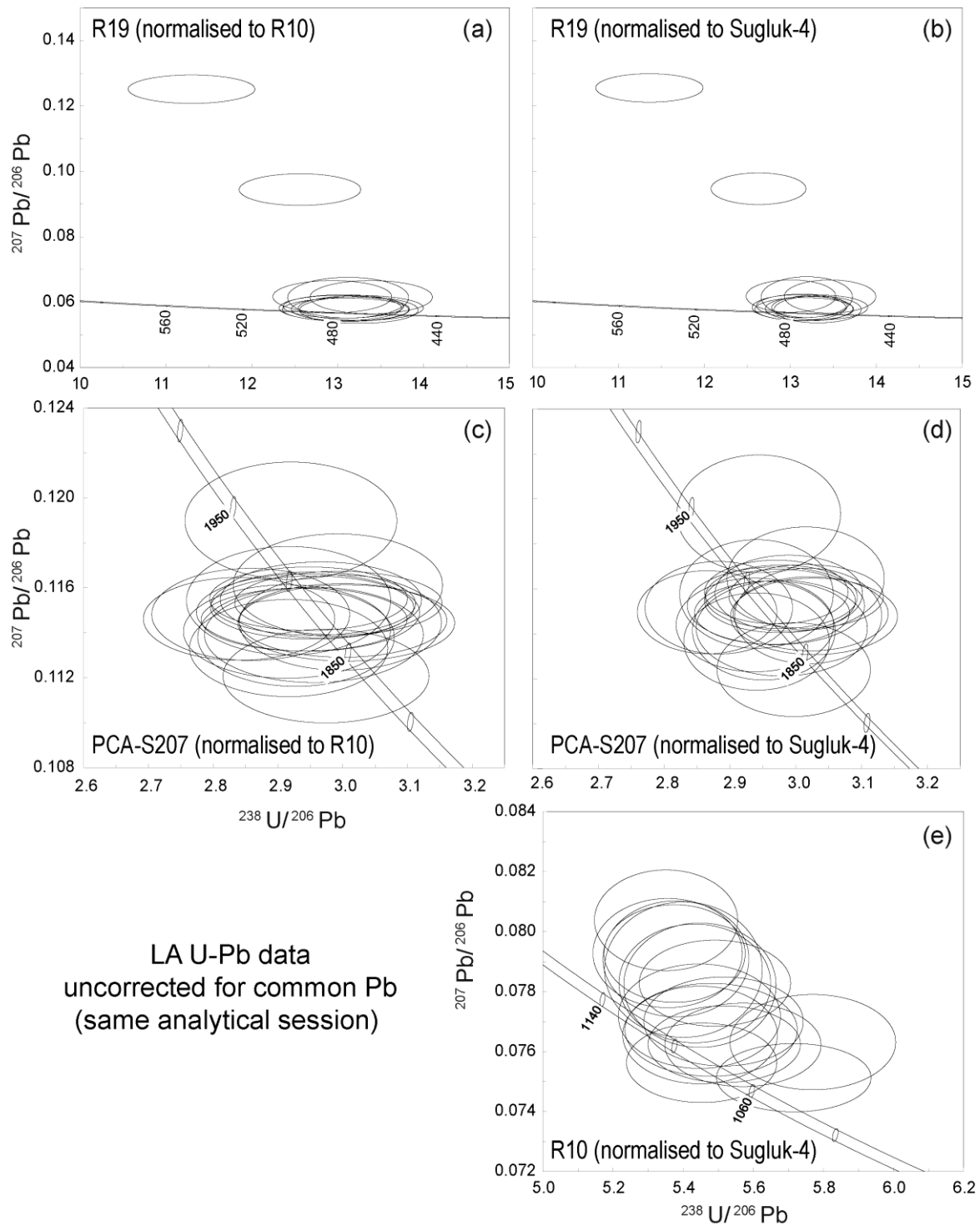


Fig. 9. Tera-Wasserburg plots of rutiles R19 (11 datapoints), PCA-S207 (20 datapoints from 3 grains) and R10 (17 datapoints). (a) R19 normalised to R10 (average of isotopic ratios from this work); (b) R19 normalised to Sugluk-4; (c) PCA-S207 normalised to R10 (average of isotopic ratios from this work); (d) PCA-S207 normalised to Sugluk-4; (e) R10 normalised to Sugluk-4. All LA U-Pb data uncorrected for common Pb and obtained during the same analytical session.

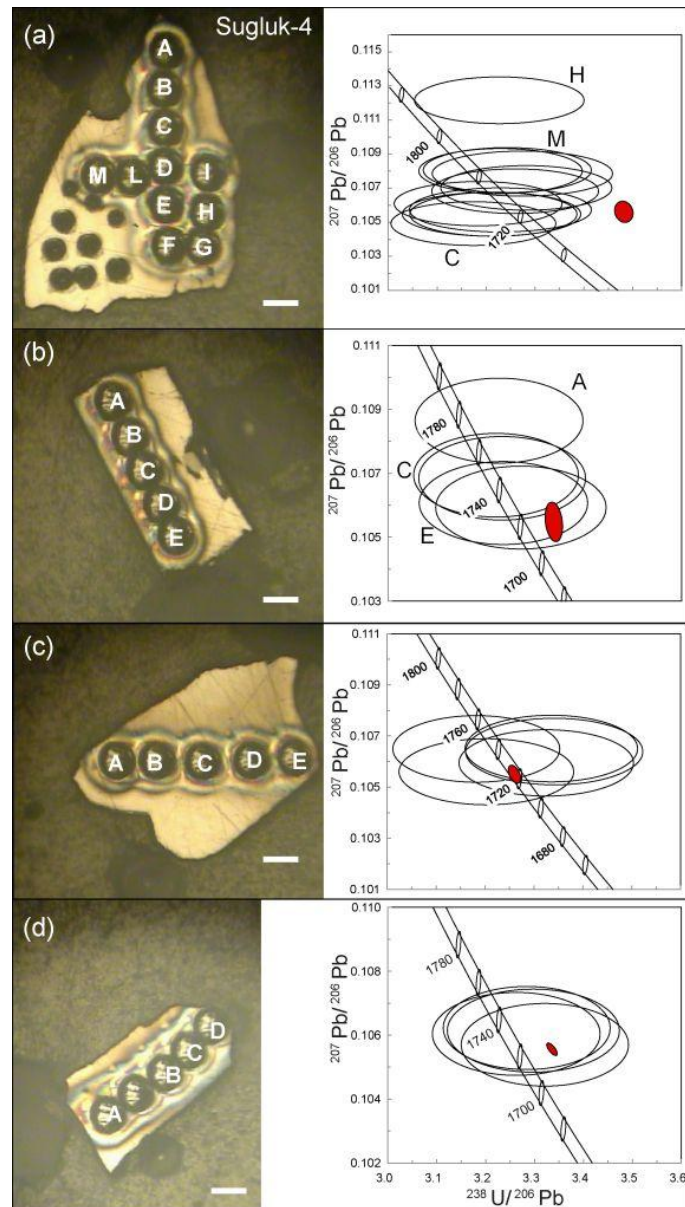


Fig. 10. Tera-Wasserburg diagrams of Sugluk-4 rutile grains analysed by both ID-TIMS (filled ellipses) and LA-MC-ICP-MS (open ellipses), the latter normalised to R10; the U-Pb ID-TIMS data are corrected for common Pb. The weighted average of the $^{207}\text{Pb}/^{206}\text{Pb}$ dates (LA data) is: 1741 ± 14 Ma, grain r1 (a); 1747 ± 23 , grain r2 (b); 1735.0 ± 8.6 , grain r3 (c); 1732.2 ± 4.5 grain r4 (d), while the $^{207}\text{Pb}/^{206}\text{Pb}$ ID-TIMS date for each grain is 1726.6 ± 8.7 Ma (r1), 1724.4 ± 8.5 Ma (r2), 1723.7 ± 4.9 Ma (r3) and 1723.8 ± 2.8 (r4). Grain r1 shows the larger scatter of ratios, and includes one of the 14 datapoints (spot H) with the highest relative common Pb content of the whole dataset (positive tail of the probability density distribution of Fig. 6). In all images the white scale bar is $50 \mu\text{m}$.

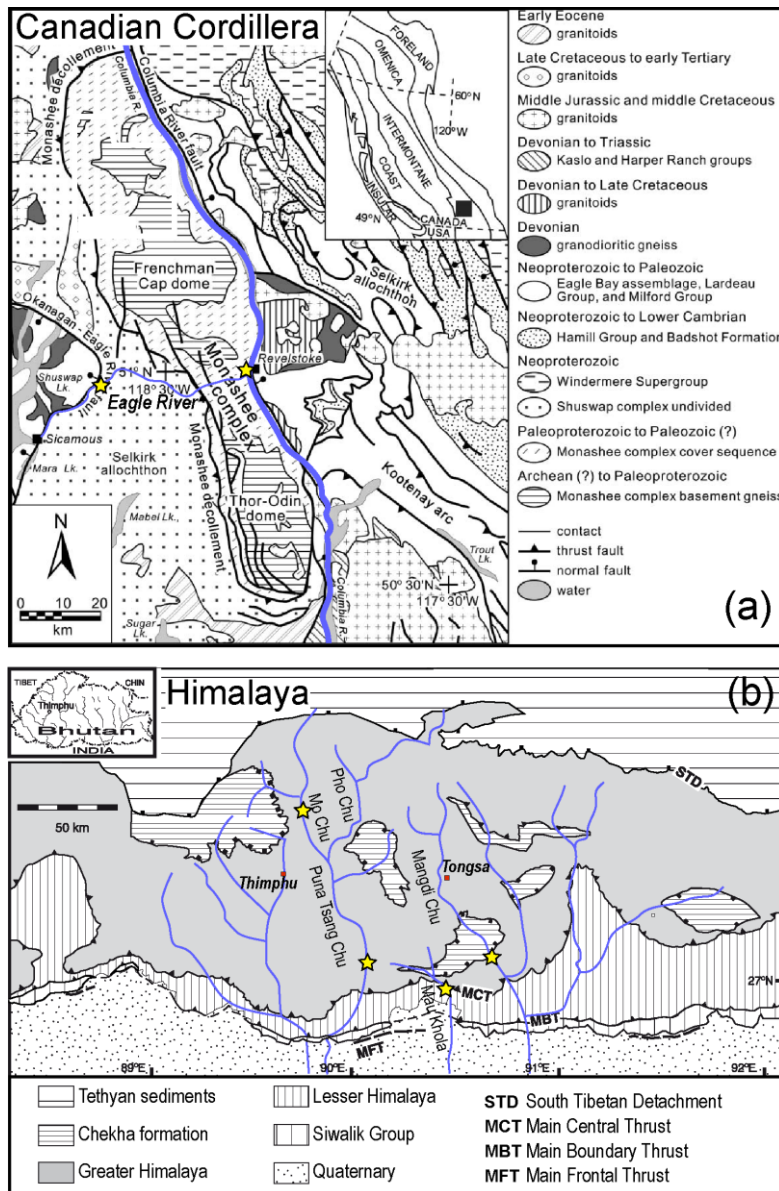


Fig. 11. Schematic geological maps of a portion of the Canadian Cordillera in British Columbia (a) and of the Bhutan Himalaya (b). Stars indicate the location of detrital rutile samples from modern rivers. Maps modified after Crowley and Parrish (1999) and Hollister and Grujic (2006).

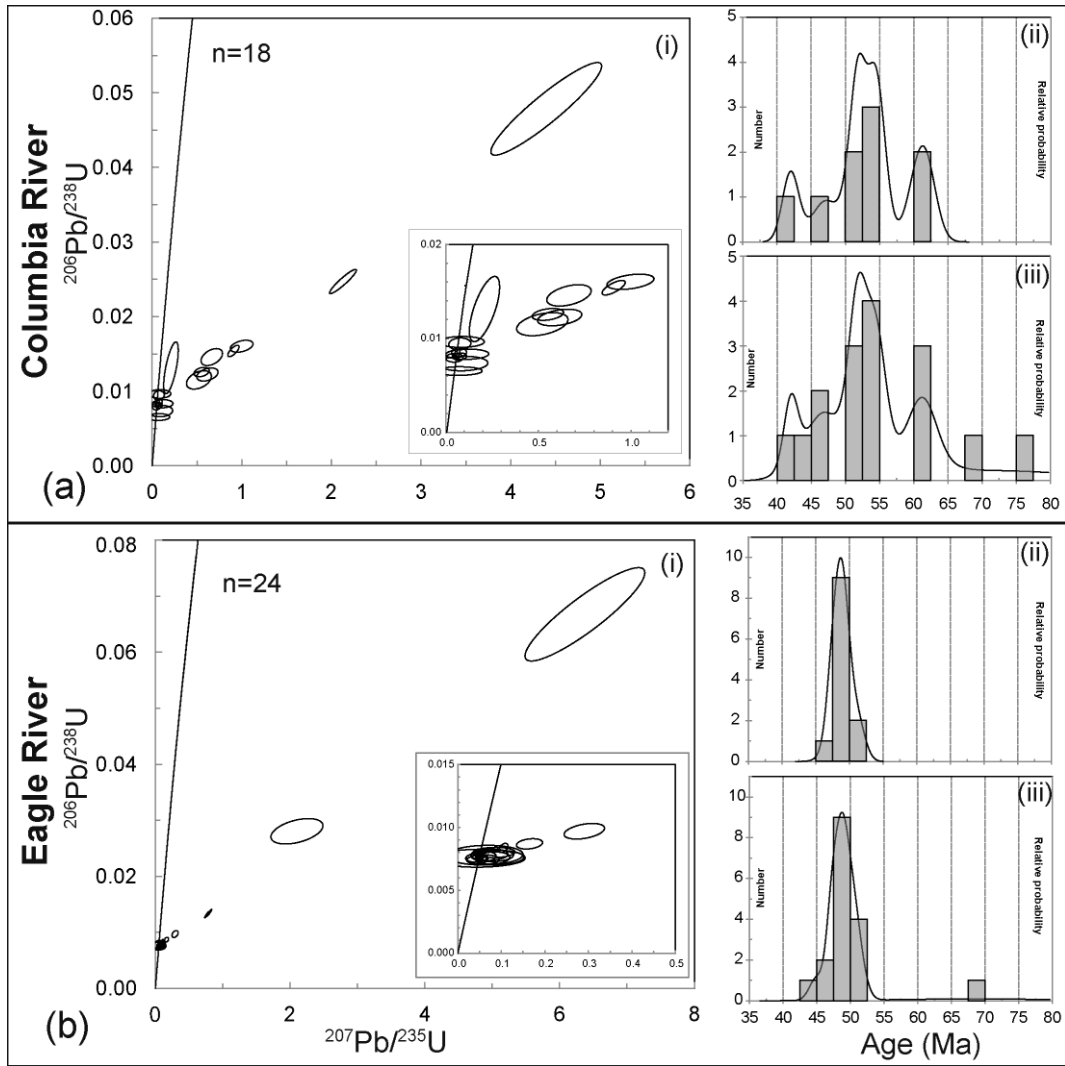


Fig. 12. U-Pb data of detrital rutile samples from British Columbia. (a) and (b) are samples BC-04g66 (Columbia River) and BC-04g67 (Eagle River) respectively, represented as Concordia diagrams (i) and as probability density plots ($^{206}\text{Pb}/^{238}\text{U}$ dates) of the concordant datapoints only (ii) and the concordant plus the originally discordant datapoints after projection (iii) as explained in the text. All data not corrected for common Pb and normalised to Sugluk-4.

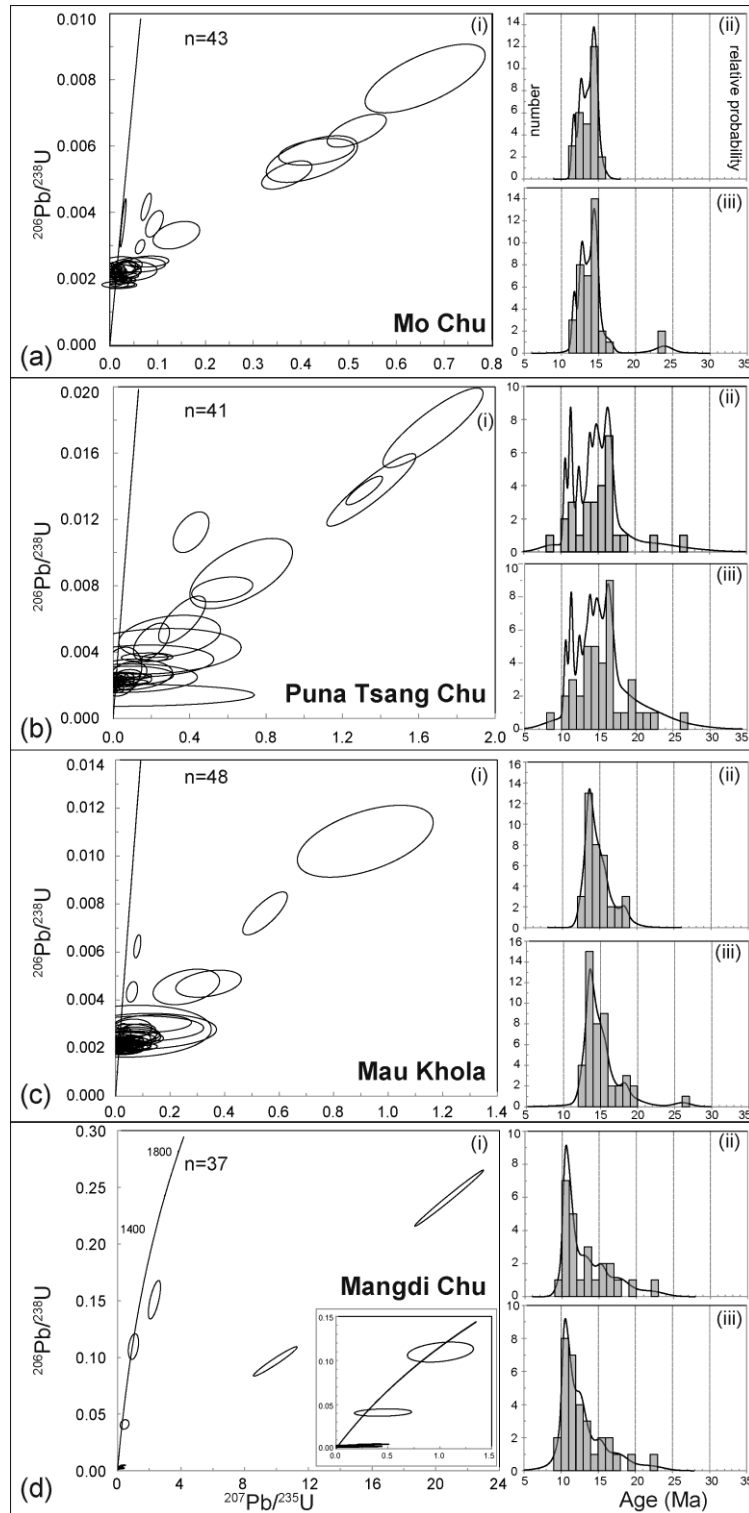


Fig. 13. U-Pb data of detrital rutile samples from Bhutan. (a), (b), (c) and (d) are samples BH0108 (Mo Chu), LB09-03 (Puna Tsang Chu), LB09-02 (Mau Khola) and LB09-01 (Mangdi Chu). The data are represented as Concordia diagrams (i) and as probability density plots ($^{206}\text{Pb}/^{238}\text{U}$ dates) of the concordant datapoints only (ii) and the concordant plus the originally discordant datapoints after projection (iii) as explained in the text. All data not corrected for common Pb and normalised to Sugluk-4.

Supplementary file

Geological and thermochronological setting of Sugluk-4 and PCA-S207

Sugluk-4 and PCA-S207 are a granulite facies quartzite from the Ungava segment of the Trans-Hudson orogen of Canada (the northern Cape Smith Belt of Quebec) and a highly strained granulite facies paragneiss from the Snowbird Tectonic Zone (East Lake Athabasca region, Saskatchewan, Canada). Many of the Paleoproterozoic orogenic belts of Canada represent collision zones between Archean provinces that amalgamated between 2.0 and 1.8 Ga (Hoffman, 1988). One of the main crustal-scale features of the Canadian Shield is the Snowbird tectonic zone, a high amplitude linear anomaly in the horizontal gradient map of the Canadian Shield (Fig. 1 of Martel et al., 2008), which has been interpreted either as a Paleoproterozoic suture reflecting the <1.9 Ga collision of the Rae and Hearne Archean provinces or an intracontinental Archean shear zone with only limited Paleoproterozoic reworking (Hoffman, 1988; Hanmer et al., 1995). Recent work in this area documented the importance of 1.9 Ga metamorphism and subsequent exhumation of deep-crustal rocks (Baldwin et al., 2004; Mahan et al., 2006; Flowers et al., 2006a; 2008; Martel et al., 2008; Dumond et al., 2008). The East Lake Athabasca region spans the central segment of the Snowbird tectonic zone, and exposes a broad area of high P granulites (1.0 to >1.5 GPa and > 750°C). The region has been effectively shielded from major perturbation since the Proterozoic. PCA-S207 is from the southern domain (Fig. 2 of Flowers et al. 2006a; cf. “upper deck” of Hanmer et al., 1994) of the East Athabasca Mylonite triangle, a region exhumed between the ~ 1.9 Ga high-pressure granulite facies metamorphism and the ~ 1.7 Ga unconformable deposition of Athabasca basin sediments on the exhumed rocks, as constrained by synkinematic monazite from shear zones dated at 1.85 Ga (Mahan et al., 2006; Flowers et al., 2006a). Single grain ID-TIMS U-Pb thermochronological data in the range 1.7–1.8 Ga have been obtained for titanite, apatite and rutile from the different lithotectonic domains of the East Lake Athabasca region, reflecting cooling through temperatures of ~ 650–450 °C (Baldwin et al., 2004; Flowers et al., 2006a). $^{40}\text{Ar}/^{39}\text{Ar}$ muscovite and biotite dates from 1.78 ± 0.01 to 1.72 ± 0.01 Ga and (U-Th)/He zircon dates from 1.73 ± 0.01 to 1.72 ± 0.01 Ga record final cooling through 350–300 °C and < 180 °C, respectively (Flowers et al., 2006a, 2006b).

Within the Canadian Shield, the Trans-Hudson orogen is the most completely preserved Paleoproterozoic collisional belt formed between 2.0 and 1.8 Ga ago following the closure of the Manikewan Ocean that was interposed between the Rae craton and the Superior craton

(Hofmann, 1988; St-Onge et al., 2001; Corrigan et al., 2009). The Ungava segment of this orogen is a ~ 400 km long belt preserving metaplutonic and metasedimentary thrust sheets (the Narsajuaq arc and Cape Smith belt, Fig. 1 of St-Onge et al., 2000) accreted to the Archean rocks of the Superior craton to the south (Lucas et al., 1992; Machado et al., 1993). In the vicinity of Sugluk Inlet on the north coast of the Ungava peninsula (Fig. 1 of Parrish, 1989) a sheared tectonic assemblage of igneous and metasedimentary rocks belonging to the Narsajuaq arc and Sugluk Group occurs at granulite facies conditions, with peak pressures of ~ 7–8 kbar and at >800°C (St-Onge et al., 2000). Turbiditic sedimentary rocks and the Sugluk-4 quartzite from this location yielded an assemblage of detrital zircons ranging in age from 1833–1840 Ma and 1832–1834 Ma respectively, as well as Archean zircons (ID-TIMS U-Pb data: Parrish 1989; Parrish and Noble, 2003). These zircons are interpreted as derived from the 1.82–1.84 Ga plutonic rocks of the Narsajuaq arc. Metamorphic overgrowths at 1825–1829 Ma on zircon cores older than 2230 Ma in a garnet-bearing orthogneiss relate to the granulite facies metamorphism accompanied by strong deformation that followed the deposition of the sedimentary rocks. A few Sugluk-4 concordant zircon rim U-Pb dates as young as 1813 ± 9 Ma have also been recently obtained by LA-MC-ICP-MS (Bracciali, unpublished data). Monazite and xenotime from sample Sugluk-3 (a garnet-bearing orthogneiss) 1815–1820 Ma and 1792 Ma old suggest a protracted period of slow-cooling from high metamorphic grade to at least 1758 Ma, the age of igneous zircons from a granitic dyke cross-cutting all the elements of the orogen.

References

- Baldwin, J.A., Bowring, S.A., Williams, M.L. and Williams, I.S., 2004. Eclogites of the Snowbird tectonic zone: petrological and U-Pb geochronological evidence for Paleoproterozoic high-pressure metamorphism in the western Canadian Shield. *Contributions to Mineralogy and Petrology* 147, 528-548.
- Corrigan, D., Pehrsson, S., Wodicka, N. and de Kemp, E., 2009. The Palaeoproterozoic Trans-Hudson Orogen: a prototype of modern accretionary processes. *Geological Society, London, Special Publications* 327, 457-479.
- Dumond, G., McLean, N., Williams, M.L., Jercinovic, M.J. and Bowring, S.A., 2008. High-resolution dating of granite petrogenesis and deformation in a lower crustal shear zone: Athabasca granulite terrane, western Canadian Shield. *Chemical Geology* 254, 175-196.
- Flowers, R.M. et al., 2006a. Multistage exhumation and juxtaposition of lower continental crust in the western Canadian Shield: Linking high-resolution U-Pb and $^{40}\text{Ar}/^{39}\text{Ar}$ thermochronometry with pressure-temperature-deformation paths. *Tectonics* 25, TC4003.

- Flowers, R.M., Bowring, S.A., Reiners, P.W., 2006b. Low long-term erosion rates and extreme continental stability documented by ancient (U-Th)/He dates. *Geology* 34, 925-928.
- Flowers, R., Bowring, S., Mahan, K., Williams, M., Williams, I., 2008. Stabilization and reactivation of cratonic lithosphere from the lower crustal record in the western Canadian shield. *Contributions to Mineralogy and Petrology* 156, 529-549.
- Hanmer, S., Parrish, R., Williams, M. and Kopf, C., 1994. Striding-Athabasca mylonite zone: Complex Archean deep-crustal deformation in the East Athabasca mylonite triangle, northern Saskatchewan. *Canadian Journal of Earth Sciences* 31, 1287-1300.
- Hanmer, S., Williams, M. and Kopf, C., 1995. Modest movements, spectacular fabrics in an intracontinental deep-crustal strike-slip fault: Striding-Athabasca mylonite zone, NW Canadian Shield. *Journal of Structural Geology* 17, 493-507.
- Hoffman, P.F., 1988. United Plates of America, The Birth of a Craton: Early Proterozoic Assembly and Growth of Laurentia. *Annual Review of Earth and Planetary Sciences* 16, 543-603.
- Lucas, S.B., St-Onge, M.R., Parrish, R.R. and Dunphy, J.M., 1992. Long-lived continent-ocean interaction in the Early Proterozoic Ungava orogen, northern Quebec, Canada. *Geology* 20, 113-116.
- Machado, N., David, J., Scott, D.J., Lamothe, D., Philippe, S. and Gariépy, C., 1993. U-Pb geochronology of the western Cape Smith Belt, Canada: new insights on the age of initial rifting and arc magmatism. *Precambrian Research* 63, 211-223.
- Mahan, K., Williams, M., Flowers, R., Jercinovic, M., Baldwin, J. and Bowring, S., 2006. Geochronological constraints on the Legs Lake shear zone with implications for regional exhumation of lower continental crust, western Churchill Province, Canadian Shield. *Contributions to Mineralogy and Petrology* 152, 223-242.
- Martel, E., van Breemen, O., Berman, R.G. and Pehrsson, S., 2008. Geochronology and tectonometamorphic history of the Snowbird Lake area, Northwest Territories, Canada: New insights into the architecture and significance of the Snowbird tectonic zone. *Precambrian Research* 161, 201-230.
- Parrish, R.R., 1989. U-Pb geochronology of the Cape Smith Belt and Sugluk block, northern Quebec. 1989.
- Parrish, R.R. and Noble, S.R., 2003. Zircon U-Pb geochronology by isotope dilution – thermal ionisation mass spectrometry (ID-TIMS). In: J.M. Hancher and P.W.O. Hoskin (Eds.): *Reviews in Mineralogy and Geochemistry*. Mineralogical Society of America and Geochemical Society., pp. 183-213.

St-Onge, M.R., Wodicka, N. and Lucas, S.B., 2000. Granulite- and amphibolite-facies metamorphism in a convergent-plate-margin setting: synthesis of the Quebec-Baffin segment of the Trans-Hudson Orogen. *The Canadian Mineralogist* 38, 379-398.

St-Onge, M.R., Scott, D.J. and Wodicka, N., 2001. Terrane boundaries within Trans-Hudson Orogen (Quebec-Baffin segment), Canada: changing structural and metamorphic character from foreland to hinterland. *Precambrian Research* 107, 75-91.